# MASTERARBEIT | MASTER'S THESIS

Titel | Title

Pharmacological characterization of new psychoactive substances

verfasst von | submitted by

Ronald Derndorfer BSc

angestrebter akademischer Grad | in partial fulfilment of the requirements for the degree of

Magister pharmaciae (Mag. pharm.)

Wien | Vienna, 2026

| | |
|---|---|
| Studienkennzahl lt. Studienblatt \| Degree programme code as it appears on the student record sheet: | UA 066 605 |
| Studienrichtung lt. Studienblatt \| Degree programme as it appears on the student record sheet: | Masterstudium Pharmazie |
| Betreut von \| Supervisor: | ao. Univ.-Prof. Dr. Harald Sitte |

# Declaration

I hereby declare that I, Ronald Derndorfer, have written this master's thesis entitled

*Pharmacological characterization of new psychoactive substances*

independently and using only the sources cited in this thesis. I did not receive any unauthorised assistance in any form. Some phrasing in this thesis was refined with the assistance of AI to improve clarity and readability. All scientific content, data interpretation, and conclusions remain the sole responsibility of the author. I have not previously submitted this master's thesis in any form in this or any other country for the achievement of an academic degree. All figures taken from the literature are properly cited. This master's thesis was discussed with and critically reviewed by MSc. Nina Kastner and Univ.-Prof. Dr. Harald Sitte prior to submission.

Vienna, May 2026

Ronald Derndorfer

## Acknowledgement

I would like to thank my supervisor, Univ.-Prof. Dr. Harald Sitte, and my lab mentor, MSc. Nina Kastner, for their continuous support, as well as for their valuable explanations and advice throughout this master's thesis. They guided and supported me throughout the entire process. Furthermore, I would like to thank Julia Bicher, Marion Holy and Fatemeh Kooti for their support in the laboratory, particularly regarding practical work and training in good laboratory practice. I also thank all other members of the laboratory for their assistance.

Special thanks go to my parents, my sister, my uncle Peter, and my aunt Regina, who supported me in many different ways along my path. In addition, I would like to thank my close friends Lukas, Evelyn, Philipp, Bernhard, Julian, and Biko, who stood by my side at different stages of my life and inspired me. Thank you all. It has been an exciting journey so far, and I look forward to what lies ahead for all of us!

Ronald

# Abstract

New psychoactive substances have gained increasing attention in public health and may also provide therapeutic options for psychiatric and cognitive disorders. MDMA is currently in Phase III clinical trials as an adjunct to psychotherapy for the treatment of PTSD. Despite two Phase III studies, the FDA issued a Complete Response Letter requesting additional studies to further evaluate safety and efficacy. This has driven the development of MDMA analogues with potentially improved pharmacological profiles.

In this master's thesis, six benzofuran cathinone derivatives were investigated *in vitro* for their activity at the monoamine transporters SERT, DAT, and NET using uptake inhibition and superfusion release assays in HEK-293 cells. $IC_{50}$ values and release properties were determined. The results indicated that stereochemistry, the position of the substituent on the benzofuran and the alkyl-chain length influence $IC_{50}$ values. Potency varied among the transporters with the highest potency at DAT, intermediate at NET, and the lowest at SERT. Release experiments showed that all substances induced release at SERT. At DAT, only *R*-βK-6-MAPB showed release, whereas at NET, both stereoisomers of βK-6-MAPB exhibited release.

These findings indicate that some of the tested benzofuran cathinones may offer selective serotonergic activity, highlighting their potential as candidates for further pharmacological evaluation for PTSD.

# Table of Contents


Declaration ..... i
Acknowledgement ..... iii
Abstract ..... v
List of Figures ..... vii
List of Abbreviations ..... ix
1 Introduction ..... 1
1.1 Monoamine neurotransmitters and their transporters ..... 1
1.2 Amphetamines ..... 4
1.2.1 Amphetamine analogues ..... 6
1.2.1.1 Classical (unsubstituted) amphetamines ..... 6
1.2.1.2 Substituted amphetamines ..... 6
1.2.1.3 Cathinones (β-keto amphetamines) ..... 8
1.2.1.4 Benzofuran derivatives ..... 9
1.2.2 Therapeutic use of amphetamines ..... 11
1.3 Introduction to cell lines and *in vitro* assays ..... 11
2 Materials and methods ..... 13
2.1 Investigated compounds ..... 13
2.2 Cell culture ..... 14
2.3 *In vitro* uptake inhibition assay ..... 14
2.4 Release assay ..... 16
3 Results ..... 18
3.1 Uptake inhibition assay ..... 18
3.2 Screening for releasing activity ..... 21
3.3 Concentration-response analysis of releasing compounds ..... 25
4 Discussion ..... 28
5 Conclusion ..... 33
6 References ..... 34
7 Appendix ..... 47
7.1 Zusammenfassung ..... 47

# List of Figures

**Figure 1: Structural definition of amphetamines according to Biel and Bopp:(i) an unsubstituted phenyl ring, (ii) a two-carbon side chain between the phenyl ring and nitrogen, (iii) an α-methyl group, and (iv) a primary amino group (27). ..... 4**

**Figure 2: Mechanistic insights into amphetamine action. Adapted from Sitte & Freissmuth, Trends Pharmacol Sci. 2014; 36(1):41–50. doi: 10.1016/j.tips.2014.11.006..... 6**

**Figure 3: Chemical structures of selected subgroups of amphetamine derivatives. In this case R1 and R2 represent halogens (F, Cl, Br and I)..... 10**

**Figure 4: Overview of the tested compounds, including their abbreviations, IUPAC names, structural formulas and molecular masses..... 13**

**Figure 5: Pre-incubation time, uptake time and the blockers used for the uptake inhibition assay. ..... 15**

**Figure 6: Representation of the uptake inhibition curves. The x-axis shows the molar concentration of the tested compounds and the y-axis indicates the percentage uptake of the radiolabeled substrate. Above the graphs, the corresponding MAT to which both curves correspond is indicated. The data points are the mean ± standard deviation (SD) from three indipendent experiments, each performed in triplicate. To determine the half-maximal inhibitory concentration (IC50), the experimental data were plotted and fitted using non-linear regression with a sigmoidal dose-response curve..... 19**

**Figure 7: Overview of the results from the uptake inhibition assays. The graph shows the tested compounds, including their chemical structures and $IC_{50}$ values for the respective MATs. ..... 20**

**Figure 8: Release of preloaded [$^3$H]-5-HT or [$^3$H]-$MPP^+$ in HEK-293 cells via stably expressing SERT, DAT or NET: Each graph shows the release profile of [$^3$H]-5-HT at SERT (A-F), of [$^3$H]-$MPP^+$at DAT (G-L) or NET (M-R) of a compound with and without MON in the superfusion release assay. The x-axis represents the time elapsed since the start of the experiment, and the y-axis displays the percentage of radiolabeled substrate released every two minutes. Compounds were applied between 14 and 24 min at concentrations near their respective $IC_{50}$ values either in KHB (dashed line) or in the presence of 10 µM MON in KHB (solid line). Values represent the mean ± SD of 3 independent cell culture preparations (n = 3), performed in triplicate. Statistical significance between KHB and MON conditions at the indicated time points was assessed using a mixed-effects model with Šidák correction for multiple comparisons, confirming the releasing activity of the tested compounds. Control experiments included the known full releaser pCA for SERT and S-AMPH for DAT and NET. Differences were considered**

**statistically significant at $p < 0.05$. Symbols indicate significance levels as follows: *$p < 0.05$, **$p < 0.01$, ***$p < 0.001$ and ****$p < 0.0001$. ..... 23**

**Figure 9: Overview of the results from the superfusion release assays. The table shows the tested compounds, including their structural formulas, and indicates whether they elicit a release effect at each MAT, allowing classification as releasers. ..... 24**

**Figure 10: Release of preloaded [$^3$H]-substrate in HEK-293 cells stably expressing MAT. Each graph shows the release profile of [$^3$H]-substrate for a single compound in the superfusion release assay at one MAT. The x-axis represents the logarithmic molar concentration of the compound, while the y-axis displays the percentage of radiolabeled substrate released relative to the control substance. Values represent the mean ± SD of three independent cell culture preparations (n = 3), each performed in triplicate. Control experiments included the known full releaser for the respective MAT. ..... 26**

**Figure 11: Concentration-response curve results from the superfusion release assay, showing each tested compound with its corresponding transporter, potency ($EC_{50}$), efficacy ($E_{max}$) and release percentage relative to a standard full releaser (pCA for SERT and S-AMPH for DAT and NET). ..... 27**

**Figure 12: Uptake inhibition effects of benzofuran cathinones at MATs. An upward arrow indicates an increase in $IC_{50}$, whereas a downward arrow indicates a decrease. The number of arrows reflects the magnitude of the effect: more arrows correspond to a stronger influence. The effect of stereochemistry is indicated above the chiral carbon. A gray arrow indicates an uncertain effect, while black arrows indicate more likely effects. ..... 30**

**Figure 13: Effects of structural features of benzofuran cathinones on their release efficacy ($E_{max}$) at MATs. The effect of stereochemistry is indicated above the chiral carbon atom. Yellow-circled areas highlight the key structural features necessary to elicit a release effect at MATs. ..... 32**

**Notice regarding image rights:**

I have made every reasonable effort to identify all copyright holders of the images used in this thesis and to obtain permission for their use where required. Should any copyright infringement nevertheless come to light, I kindly request that I be notified accordingly

# List of Abbreviations

| | |
|---|---|
| [$^3$H]-5-HT | Tritium-labelled 5-hydroxytryptamine (serotonin) |
| [$^3$H]-MPP$^+$ | Tritium-labelled 1-methyl-4-phenylpyridinium |
| ADHD | Attention Deficit/Hyperactivity Disorder |
| *S*-AMPH | *S*-(+)-amphetamine |
| DMEM | Dulbecco′s Modified Eagle′s Medium |
| DAT | Dopamine transporter |
| DOx | 4-substituted-2,5-dimethoxyamphetamines |
| FBS | Fetal bovine serum |
| HEK-293 | Human Embryonic Kidney 293 cells |
| hNET | Human norepinephrine transporter |
| KHB | Krebs-HEPES buffer |
| LDX | Lisdexamfetamine |
| LSD | Lysergic acid diethylamide |
| MAO | Monoamine oxidase |
| MAT | Monoamine transporter |
| MDA | 3,4-methylenedioxyamphetamine |
| MDMA | 3,4-methylenedioxymethamphetamine |
| METH | Methamphetamine |
| MON | Monensin |
| NPS | New psychoactive substances |
| *p*CA | Para-chloroamphetamine |
| PDL | Poly-D-lysine |
| PTSD | Post-traumatic stress disorder |
| SERT | Serotonin transporter |
| SLC6 | Solute carrier family 6 |
| SOI | Substance of interest |
| SSRI | Selective serotonin reuptake inhibitor |
| TAAR1 | Trace amine-associated receptor 1 |
| VMAT | Vesicular monoamine transporter |

# 1 Introduction

## 1.1 Monoamine neurotransmitters and their transporters

Monoaminergic neurotransmitters such as serotonin, dopamine, and noradrenaline are involved in neuronal signaling in the human brain (1). Their extracellular levels are primarily regulated by monoamine transporters (MATs), which belong to the solute carrier family 6 (SLC6). This transporter family includes the norepinephrine transporter (NET/SLC6A2), dopamine transporter (DAT/SLC6A3), and serotonin transporter (SERT/SLC6A4; 2,3). MATs are membrane-expressed proteins located at presynaptic terminals in the perisynaptic region (4), where they mediate the reuptake of neurotransmitters from the synaptic cleft following synaptic transmission (5). By removing released neurotransmitters from the extracellular space into neurons and glial cells, MATs contribute to neurotransmitter homeostasis and modulate both the duration and intensity of monoaminergic signaling (1).

The crucial physiological role of MATs is highlighted by their association with various neuropsychiatric and neurological disorders. Serotonergic signaling is closely linked to mood regulation, and altered SERT function has been implicated in depression and anxiety disorders (6,7). Dopaminergic signaling contributes to motivation, movement, mood, and learning, while dysfunction of DAT is associated with ADHD, Parkinson's disease, and substance abuse (8,9). Noradrenergic signaling is involved in cognition and emotional processing, and its dysregulation is associated with cognitive and affective disorders (10). Therefore, MATs are prominent pharmacological targets for antidepressants, psychostimulants, and various neuroactive drugs such as cocaine and amphetamines (1).

Structurally, all MATs share a conserved architecture composed of 12 α-helical transmembrane domains connected by intracellular and extracellular loops. Both the N- and C-termini are located on the intracellular side of the membrane. The transporters contain a primary high-affinity substrate-binding site (S1), where one substrate molecule binds together with one or two $Na^+$ ions. Within the S1 site, a hydrophobic region interacts with the aromatic moiety of the substrate, while a hydrophilic region contains a conserved aspartate residue that facilitates ionic interaction with the protonated amino group of the monoamine (5). In addition to the primary S1 site, a second binding site (S2) has been identified in SERT and NET (10). These structural features enable the conformational transitions that drive substrate transport.

Transport by MATs follows the alternating access model, in which conformational changes alternately expose the central binding site to either the extracellular or intracellular side of the membrane. In the outward-facing conformation, the S1 site is accessible to substrate and $Na^+$

binding. Substrate binding then triggers conformational transitions that lead to closure of the extracellular gate. Subsequently, the intracellular gate opens, resulting in an inward-facing conformation that enables release of the substrate into the cell. Hydration of the substrate-binding site facilitates this transition. After uptake, monoamines are either repackaged into synaptic vesicles for subsequent release or metabolized by monoamine oxidase (MAO) (5). Monoamine uptake and release by MATs are further influenced by the ionic environment surrounding the neurons. Monoamine uptake occurs through secondary active transport coupled to $Na^+$ and $Cl^-$. All MATs contain two conserved $Na^+$ binding sites (Na1 and Na2) and one conserved $Cl^-$ binding site (10). Extracellular $Na^+$, present at higher concentrations outside the cell, stabilizes the outward-facing conformation of the transporter (11). The $Na^+$ gradient that drives substrate uptake is maintained by the $Na^+/K^+$-ATPase. Since monoamines are transported in their protonated form, substrate binding and transport strongly depend on electrostatic interactions (2,12). In addition to $Na^+$ and $Cl^-$ ions, transporter activity is further influenced by intracellular $K^+$. The return of SERT from the inward-facing to the outward-facing state constitutes the rate-limiting step of the transport cycle and is facilitated by cytoplasmic $K^+$ (6). In the presence of a substrate, SERT predominantly adopts the inward-facing conformation, as the transition from the inward- to the outward-facing state is slower than the reverse transition (6,13), whereas in the absence of substrate, SERT favors the outward-facing conformation (14). Under certain conditions, intracellular $H^+$ can substitute for $K^+$, particularly in the presence of a transmembrane pH gradient that promotes uptake (6). Although a distinct $K^+$ binding site has not been conclusively identified (10), recent studies indicate that DAT can also use $K^+$ as a catalytic ion, while it is not essential for transport. Likewise, NET can also interact with $K^+$ at the Na1 site under certain conditions (10). Taken together, these observations underline the dynamic ion dependence of MAT-mediated transport.

Transporter function is regulated not only by ions but also by the lipid composition of the plasma membrane. Cholesterol, a key component of the membrane, contributes to modulating the conformational dynamics of MATs. Cholesterol depletion shifts MATs toward an inward-facing conformation, as shown for DAT (15–17) and SERT (18,19). Beyond these conformational effects, MATs can form higher-order oligomeric structures within the membrane, which contribute to the regulation and quality control of transporter function. In this context, altered cholesterol levels have been associated with several psychiatric disorders (20). Accordingly, MATs play a central role in regulating key monoamines in neuronal signaling.

While MATs regulate extracellular monoamine levels through reuptake at the plasma membrane, intracellular monoamine storage depends on vesicular monoamine transporters

(VMATs). VMATs are membrane proteins located in synaptic vesicles that mediate the sequestration of monoaminergic neurotransmitters. In neurons, VMAT2 (SLC18A2) is the predominant isoform (21–23). VMAT2 operates as a proton-monoamine antiporter that exchanges two protons ($H^+$) from the vesicular lumen into the cytosol for one cationic monoamine (24). The proton gradient driving this process is generated by vesicular V-type $H^+$-ATPases (25). By regulating intracellular monoamine storage and availability, VMAT2 plays a key role in neurotransmission. Amphetamines act as substrates of VMAT2, and this interaction substantially contributes to their overall effect on monoamine release (2). Alterations in VMAT2 activity have been associated with the neurotoxic effects of amphetamines, particularly through dysregulated dopamine handling (26).

## 1.2 Amphetamines

Amphetamines can be defined from different perspectives. From a chemical standpoint, Biel and Bopp defined amphetamines as compounds characterized by four structural features: (i) an unsubstituted phenyl ring, (ii) a two-carbon side chain linking the phenyl ring to a nitrogen atom, (iii) an α-methyl group, and (iv) a primary amino group (27).

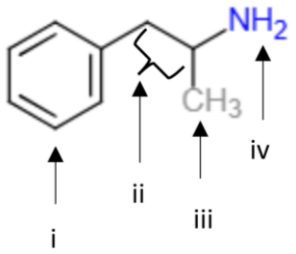


*Figure 1: Structural definition of amphetamines according to Biel and Bopp:(i) an unsubstituted phenyl ring, (ii) a two-carbon side chain between the phenyl ring and nitrogen, (iii) an α-methyl group, and (iv) a primary amino group (27).*

The term "amphetamine" is derived from α-methylphenethylamine (28). However, this chemical definition is relatively strict, as several amphetamine-related compounds, including methamphetamine (METH) and ephedrine, do not fulfill the primary amine requirement despite sharing similar pharmacological properties (2). Conversely, a purely operational definition based on molecular targets is also insufficient, since amphetamines can exert diverse effects, including inhibition of neurotransmitter reuptake and induction of neurotransmitter release (2). The primary molecular targets of amphetamines are MATs (29). Unsubstituted amphetamines generally exhibit higher potency at catecholamine transporters, particularly NET, while displaying lower potency at SERT (30). Structural modifications, especially substitutions on the phenyl ring, strongly influence transporter selectivity and pharmacological activity. Ring substitutions typically increase binding affinity for SERT (31). For example, *para*-chloroamphetamine (*p*CA) and fenfluramine display greater selectivity for SERT than DAT, whereas *S*-(+)-amphetamine (*S*-AMPH) preferentially targets DAT. Amphetamines enter monoaminergic neurons either through passive diffusion across the plasma membrane or via transporters such as SERT, DAT, and NET (32). Once inside the cell, they can subsequently enter synaptic vesicles through VMAT2-mediated transport (28). Since VMAT2 activity depends on the acidic vesicular environment, vesicular uptake of amphetamines is strongly influenced by proton gradients (28). This process represents a key step in the mechanism of action of amphetamines and forms the basis of the weak base hypothesis.

The weak base hypothesis proposes that amphetamines, which are weak bases (pKa ≈ 8-10), can passively diffuse across the vesicular membrane in their neutral form, independently of

transporter-mediated uptake. Once inside the vesicle, they become protonated, leading to vesicular alkalization and reduced membrane permeability. As a consequence, VMAT function becomes impaired, promoting the accumulation of monoamines within the cytosol (28). However, this hypothesis alone cannot fully explain amphetamine action, since stereospecific differences have been observed. For instance, *S*-(+)-METH induces vesicular monoamine release more effectively than *R*-(-)-METH. Therefore, passive diffusion is best regarded as complementary to the classical substrate-mediated VMAT transport (33). In addition to their effect on MATs and VMATs, amphetamines also affect intracellular monoamine metabolism.

Amphetamines are not primarily metabolized by monoamine oxidase (MAO) (28,34), but they can inhibit MAO activity, thereby reducing monoamine degradation and increasing cytosolic monoamine levels (2). In addition, MAO-A exhibits stereoselectivity toward AMPH, with higher affinity for the *S*-enantiomer than for the *R*-enantiomer (35,36). However, the affinity of amphetamines for MAO is substantially lower than for MATs (28). The resulting increase in cytosolic monoamine availability contributes to reverse monoamine transport mediated by MATs.

Several mechanisms have been proposed to explain transporter-mediated reverse transport. Amphetamines increase the rate of outward-to-inward transporter translocation, thereby increasing the likelihood that intracellular dopamine binds to the transporter and is subsequently released into the extracellular space (28). In addition, reverse transport may occur through a channel-like transporter state, in which substrate efflux proceeds in an uncoupled manner, resembling ion conductance through classical ion channels (28). Intracellular $Na^+$ concentrations further increase as a consequence of AMPH-induced transport activity, which additionally promotes reverse monoamine transport via DAT (37). Second messenger signaling pathways also contribute to AMPH-mediated dopamine efflux (4). Apart from these mechanistic aspects, structural modifications of amphetamines also strongly influence transporter selectivity and releasing properties.

Many amphetamines act as more potent releasers at NET than at DAT (39). In contrast, substitutions on the phenyl ring of amphetamines enhance serotonin release via SERT (31,40). Increasing N-alkyl chain length in amphetamines, with the exception of AMPH and METH, reduces binding potency at MATs while exerting comparatively minor effects on transport inhibition (41,42). Beyond transporter-mediated effects, amphetamines also interact with additional receptor and signaling systems. In particular, amphetamines act as agonists at trace amine-associated receptor 1 (TAAR1) (43,44). Furthermore, amphetamines can activate presynaptic α2-adrenergic receptors (45) and serotonin receptors of the 5-$HT_2$ family.

Para-substituted amphetamines preferentially activate 5-$HT_{2A}$ receptors (31), whereas ring-substituted amphetamines can activate 5-$HT_{2A}$, 5-$HT_{2B}$, and 5-$HT_{2C}$ receptors (46,47).

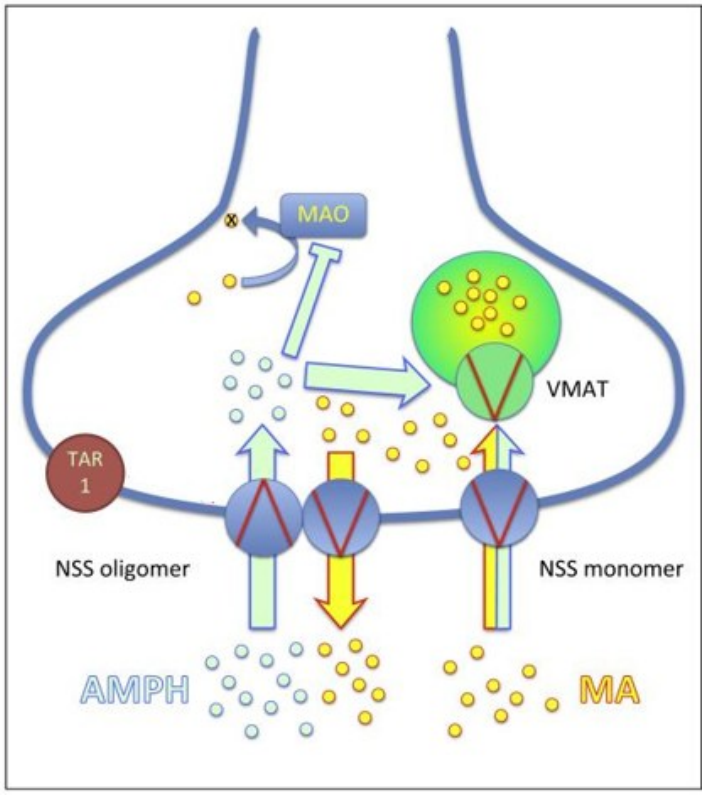


*Figure 2: Mechanistic insights into amphetamine action. Adapted from Sitte & Freissmuth, Trends Pharmacol Sci. 2014; 36(1):41–50. doi: 10.1016/j.tips.2014.11.006*

## 1.2.1 Amphetamine analogues

### 1.2.1.1 Classical (unsubstituted) amphetamines

Amphetamines are among the most commonly abused illicit substances (48). Classical amphetamines include AMPH and METH. Their pharmacological effects are primarily mediated by the release of catecholamines. Acute effects include euphoria and increased stimulation, whereas chronic or high-dose use is associated with anxiety, psychosis, and addiction (48,49).

### 1.2.1.2 Substituted amphetamines

Para-substituted amphetamines exhibit a more pronounced serotonergic profile than unsubstituted amphetamines and show increased affinity for the 5-$HT_{2A}$ receptors (31). A distinct subgroup comprises the DOx compounds (4-substituted-2,5-dimethoxyamphetamines), whose effects are primarily mediated through 5-$HT_{2A}$ receptor agonism rather than MAT interactions. Consequently, these compounds are classified as psychedelic substances with effects resembling those of classical psychedelics such as lysergic acid diethylamide (LSD) or mescaline (50).

Ring-substituted amphetamines such as MDMA and 3,4-methylenedioxyamphetamine (MDA) act as releasers at all MATs. Compared to MDMA, MDA exhibits a higher DAT/SERT ratio and stronger 5-$HT_{2A}$ agonism, which may contribute to more pronounced stimulant effects (51). MDMA is commonly described as an empathogen and entactogen, reflecting its ability to enhance prosocial behaviour, empathy, openness, and self-awareness (52). Consistent with these behavioural effects, MDMA alters emotional processing, including reduced recognition accuracy of negative emotions in women as well as enhanced emotional empathy toward positive stimuli and prosocial behaviour in men (53). These characteristic behavioural effects of MDMA are closely linked to its pharmacological actions at different targets.

MDMA acts as a substrate of all MATs, but with a particular emphasis of the SERT. MDMA induces transporter reversal at all MATs (40,54,55). At SERT, MDMA functions as a full releaser (56), whereas at DAT, MDMA induces only partial monoamine release (56). MDMA also acts as a substrate at NET, inducing transporter reversal (54). SERT-mediated serotonin release is considered a key contributor to MDMA's psychological (57) and physiological (e.g., cardiovascular) responses (58). MDMA-induced transporter reversal at NET contributes to sympathetic activation (54). This NET-mediated mechanism is thought to underlie some of the cardiovascular and psychotropic effects of MDMA (59). Overall, MDMA induces measurable monoamine release at all three MATs, with effect sizes following the order SERT > NET > DAT (56). Ring substitution reduces the DAT:SERT inhibition ratio, with 3,4-substitution causing a particularly pronounced decrease. Compared with other amphetamines, only a limited number of compounds induce release at both serotonergic and catecholaminergic systems (42,60). MDMA displays a DAT:SERT release ratio < 1 (60), and in some cases as low as 0.1 (56). Compounds with relatively higher serotonin release compared to dopamine are associated with reduced reinforcing effects in self-administration models (61). Consistent with this observation, activation of 5-$HT_{2C}$ receptors within the nucleus accumbens appears to contribute to the comparatively low abuse potential of MDMA (62). Beyond its influence on reinforcement, the pronounced serotonergic profile of MDMA is also thought to underlie its characteristic prosocial and empathogenic properties, possibly through oxytocinergic signaling pathways (63,64). Oxytocin, a neuropeptide involved in emotion recognition, prosocial behaviour (65), and altruism (66), has been implicated in several behavioural effects of MDMA. In humans, MDMA increases peripheral oxytocin concentrations (67), an effect that is likely mediated, at least in part, via 5-$HT_{1A}$ receptor activation (63). Elevated oxytocin levels are associated with enhanced sociability and subjective friendliness (64). In addition, 5-$HT_{1B}$ receptors also appear to contribute to MDMA-induced

prosocial effects (68). While serotonergic signaling contributes to both the reduced abuse potential and the prosocial effects of MDMA, interactions with adrenergic and pituitary pathways shape its physiological responses. α1- and β-adrenergic receptors are involved in the thermogenic and cardiovascular effects of MDMA (69). Besides its pharmacodynamic profile, MDMA is also characterized by distinct pharmacokinetic properties. MDMA is metabolized into several active metabolites, including 3,4-methylenedioxyamphetamine (MDA). Interindividual variability in MDMA metabolism is influenced by genetic polymorphisms, particularly in CYP2D6 (70). Many amphetamines inhibit CYP2D6, an effect that is enhanced by the 3,4-methylenedioxy substitution (71). MDMA exhibits a broad range of side effects, the severity of which depends on factors beyond dose and route of administration (72), including species (73,74), age (75,76), body temperature (77), sex (76), and genetic polymorphisms (78). Among the adverse effects, particular attention has been given to the potential neurotoxic effects of MDMA. Ring-substituted amphetamines induce degenerative changes in various rat brain regions (79). However, the doses at which potentially neurotoxic effects have been described (79) are often much higher than those that elicit relevant neurochemical, endocrine, and behavioural effects (80). A meta-analysis of 16 studies reported reduced SERT density in 8 out of 13 brain regions in human participants, many of whom were heavy MDMA users with concurrent polysubstance use. This reduction is commonly interpreted as a marker of serotonergic neurotoxicity (81). However, some studies suggest that decreases in SERT density may be at least partially reversible (82–84). While SERT density may recover after abstinence, memory-specific deficits do not appear to normalize (83). These serotonergic alterations may contribute to the cognitive deficits observed in human MDMA users. Heavy MDMA users appear to be at increased risk of impairments in executive updating, attention, and working memory (85). Regarding MDMA-related cognitive effects, cumulative lifetime exposure does not appear to be the primary determinant. Rather, the dose per session may be more critical (86). Several mechanisms have been proposed to explain MDMA-induced neurotoxicity, but their relative contributions remain unclear. It is likely that a combination of factors, including oxidative stress, toxic MDMA metabolites, mitochondrial dysfunction, glial cell involvement, excitatory events, and hyperthermia, acts synergistically to produce the observed neurotoxic effects (87).

#### 1.2.1.3 Cathinones (β-keto amphetamines)

Cathinones, also known as β-keto amphetamines, are characterized by the presence of a β-keto group (88). They form the structural basis of many designer drugs that are marketed as “bath salts” or “plant food” to evade legal control. Examples include

mephedrone (4-methylcathinone), methylone (3,4-methylenedioxymethcathinone), and MDPV (3,4-methylenedioxypyrovalerone). Synthetic cathinones are among the most frequently seized new psychoactive substances (NPS). They resemble classical psychostimulants such as amphetamine, cocaine, and MDMA in their effects (89). Although all cathinones target MATs, their mechanisms of action vary considerably. They may act as releasers, uptake inhibitors, or exhibit mixed activity by functioning as a releaser at one transporter and as an inhibitor at another. Such compounds are commonly referred to as hybrid compounds (90).

#### 1.2.1.4 Benzofuran derivatives

Aminoalkylbenzofurans and N-methylated aminoalkylbenzofurans are NPS that, similar to MDMA, act as substrates at MATs. All tested benzofurans exhibit relatively similar binding affinities for NET in the submicromolar range, suggesting psychostimulant and cardiostimulant effects comparable to those of MDMA. In contrast, their binding affinities for SERT and DAT vary considerably, resulting in DAT:SERT inhibition ratios ranging from 0.01 to 0.65. Compared with MDMA and other entactogens, which typically display ratios between 0.01 and 1, these findings suggest that benzofurans may also exhibit entactogenic effects (41). If the oxygen atom is located at the para position in benzofurans, serotonergic properties are enhanced relative to dopaminergic ones (41,91). Entactogenic effects have been reported for both para- and meta-substituted benzofurans (92–94). Although benzofurans have not been evaluated in self-administration models, compounds with higher serotonin release relative to dopamine typically show reduced reinforcing effects in such models (61). Accordingly, benzofurans, which exhibit lower DAT:SERT ratios, may have a reduced abuse potential (41). Beyond their effects on MATs, benzofurans may also interact with adrenergic and serotonergic receptors. Certain benzofurans show binding affinity for 5-$HT_{2A}$ receptors ($K_i < 1\mu M$) and display moderate functional activity ($EC_{50} \approx$ 6-13 μM; $E_{max} \approx$ 20-60%). Compared with MDMA ($K_i$ = 6.3 μM; $EC_{50}$ = 6.1 μM; $E_{max}$(MDMA) = 55%), they exhibit higher binding affinity, while functional potency and efficacy vary across compounds and are often comparable to or somewhat lower than those of MDMA (41). In contrast to MDMA, some benzofurans also exhibit a high binding affinity for 5-$HT_{2C}$ receptors ($K_i \approx$ 0.1 μM) and functional potency at 5-$HT_{2B}$ receptors ($EC_{50} \approx$ 0.1-0.3 μM) (41). Some benzofurans show high binding affinity for α2-adrenergic receptors ($K_i$ < 1 μM), which is associated with modulation of norepinephrine signaling. Interactions with α-adrenergic receptors contribute to sympathomimetic effects and may be more pronounced than those of MDMA (41). In addition to interactions with MATs and serotonergic and adrenergic receptors, TAAR1 binding

represents another mechanism through which benzofurans exert their effects. Nearly all benzofurans show strong binding affinity for TAAR1 ($K_i \approx 0.1$-1 µM), which lies within a similar range as MDMA ($K_i = 0.37$ µM). Cathinone derivatives show approximately tenfold lower affinity at TAAR1 compared with their non-keto analogues (41,42). TAAR1 is thought to mediate autoinhibitory mechanisms that limit locomotor and stimulant effects (41). These pharmacological differences may also translate into distinct toxicological and abuse-related profiles compared with MDMA.

Comparisons of structurally related compounds (e.g., MDMA vs. methylone, MBMD vs. butylone, and MDEA vs. ethylone) show that the DAT:SERT ratio increases by 6- to 41-fold, which may be associated with higher abuse liability (42). However, this stronger dopaminergic effect may be counteracted by more pronounced 5-$HT_{2C}$ receptor activity. As benzofurans exhibit higher 5-$HT_{2C}$ receptor binding, this may attenuate the reinforcing component (41). Furthermore, the increased 5-$HT_{2B}$ receptor binding affinity of benzofurans compared with MDMA (41) may be associated with an elevated risk of valvular heart disease (VHD) (46,95). For benzofuran cathinones, reduced TAAR1 affinity compared with amphetamines may result in more pronounced stimulant effects and potentially higher abuse potential (41). Some cathinones (e.g., MDMA vs. methylone) show lower VMAT2 interaction, including reduced uptake and maximal release (96,97). Since dopamine release via VMAT2 has been associated with neurotoxic effects (26), benzofuran cathinones may represent promising candidates for further investigation compared with classical benzofuran amphetamines.

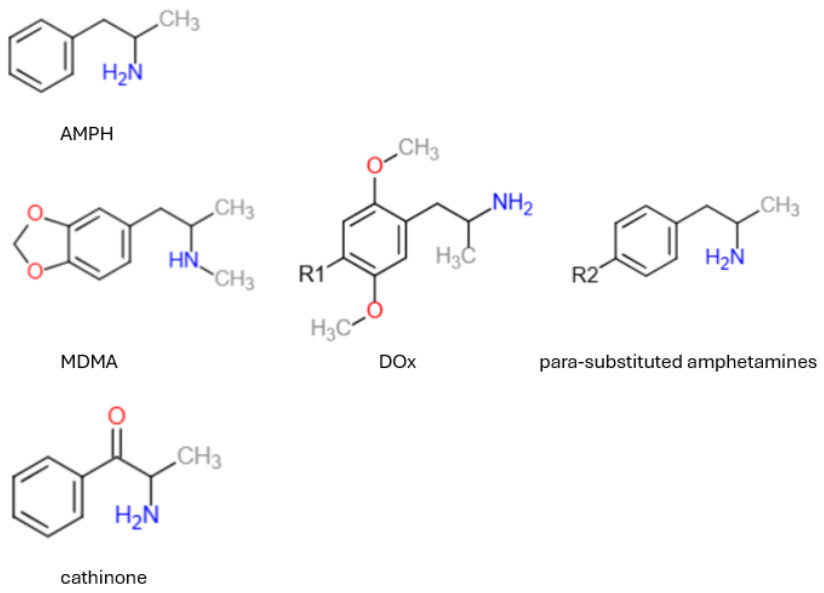


*Figure 3: Chemical structures of selected subgroups of amphetamine derivatives. In this case R1 and R2 represent halogens (F, Cl, Br and I)*

### 1.2.2 Therapeutic use of amphetamines

Amphetamines have therapeutic applications primarily in the treatment of neuropsychiatric disorders. For example, several monoaminergic drugs are used in the treatment of attention-deficit/hyperactivity disorder (ADHD). These include methylphenidate, which acts primarily as a DAT inhibitor (5), Lisdexamfetamine (LDX), a prodrug of *S*-amphetamine that functions as a monoamine-releasing agent (98), and mixed amphetamine salts containing both *S*- and *R*-amphetamine (99). Both methylphenidate and amphetamine are also used to treat narcolepsy (100). Bupropion, a cathinone derivative, is approved as a norepinephrine-dopamine reuptake inhibitor (NDRI) for the treatment of depression (101,102) and smoking cessation (103). Tranylcypromine and selegiline are also classified as amphetamines and are approved for depression (104) and Parkinson's disease (105), respectively.

Finally, MDMA shows potential for therapeutic use in post-traumatic stress disorder (PTSD). Despite the availability of multiple treatment options, treatment resistance remains high, with a non-response rate of approximately 39% (106). This underscores the need for novel therapeutic approaches for PTSD, particularly in the pharmacological domain. In recent years, an increasing number of studies have reported beneficial effects of MDMA-assisted psychotherapy in patients with PTSD (107,108). The therapeutic effects of MDMA in PTSD may be mediated by enhanced fear extinction (109,110). Furthermore, the SERT and 5-$HT_{2A}$ receptors appear to be involved in MDMA-enhanced fear extinction (109). While these findings support a role for specific receptors in fear extinction, results from animal models are not entirely consistent, highlighting the need for translation to human studies (110,111). In addition to its effects on fear extinction, MDMA may enhance its therapeutic impact in PTSD through its prosocial effects, which may facilitate patients' willingness to discuss traumatic experiences (112). These considerations have motivated the search for MDMA-like compounds with potentially improved pharmacological and toxicological profiles.

Benzofuran derivatives may differ from MDMA in their neurotoxic potential, likely due to differences in MAT and VMAT2 interactions. Therefore, this study investigates the effects of selected benzofuran cathinones on MATs (SERT, DAT, and NET), focusing on both uptake inhibition and release assays.

## 1.3 Introduction to cell lines and *in vitro* assays

For the experiments conducted in this thesis, HEK-293 cells were used due to their ease of transfection, rapid growth, and high reproducibility (113). These cells were used as a

heterologous expression system for MATs. To characterize the pharmacological properties of the investigated compounds, uptake inhibition and superfusion release assays were employed. Uptake inhibition assays measure transporter-mediated uptake of radiolabeled substrates into cells (114) and allow determination of the half-maximal inhibitory concentration ($IC_{50}$) (115). However, these assays do not distinguish between substrates (e.g., amphetamines) and non-transported competitive inhibitors (116,117). Consequently, amphetamines produce dose-dependent inhibition of uptake in these assays (117). To address this limitation, superfusion release assays were employed. These assays measure transporter-mediated substrate efflux and thereby allow differentiation between releasers and uptake inhibitors (118).

# 2 Materials and methods

## 2.1 Investigated compounds

Six compounds were examined in this study for their activity in uptake inhibition and superfusion release assays at MATs. All compounds are benzofurans. They differ in the position of the substituent on the benzofuran ring, indicated by the numbering in their names. One group carries the substituent at position 5, whereas in the other it is located at position 6. The length of the alkyl side chain was varied, with compounds predominantly containing either a propyl or a butyl group. This is reflected in the third letter of their names (P for propyl and B for butyl). All tested compounds also contain a carbonyl function in the β-position, denoted by βK (β-keto) in their names. The letter M indicates the presence of an N-methyl group, and A denotes the amino function.

| Substance | IUPAC name | Structure | M(as HCl) [g/mol] |
|---|---|---|---|
| *S*-βK-5-MABB | (*S*)-1-(benzofuran-5-yl)-2-(methylamino)butan-1-one | 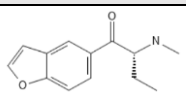 | 253.57 |
| *R*-βK-5-MABB | (*R*)-1-(benzofuran-5-yl)-2-(methylamino)butan-1-one | 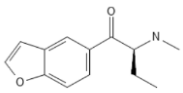 | 253.57 |
| *S*-βK-6-MABB | (*S*)-1-(benzofuran-6-yl)-2-(methylamino)butan-1-one | 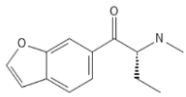 | 253.57 |
| *R*-βK-6-MABB | (*R*)-1-(benzofuran-6-yl)-2-(methylamino)butan-1-one | 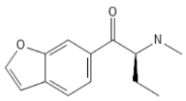 | 253.57 |
| *S*-βK-6-MAPB | (*S*)-1-(benzofuran-6-yl)-2-(methylamino)propan-1-one | 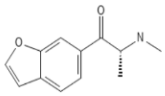 | 239.55 |
| *R*-βK-6-MAPB | (*R*)-1-(benzofuran-6-yl)-2-(methylamino)propan-1-one | 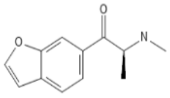 | 239.55 |

*Figure 4: Overview of the tested compounds, including their abbreviations, IUPAC names, structural formulas and molecular masses.*

The enantiopure HCl salts of the benzofuran compounds in Figure 6 were generously supplied by Dr. Matthew J. Baggot (Tactogen Inc., Palo Alto, USA). Radiolabelled tracers [$^3$H]-5-HT (NET498001MCSBR1) and [$^3$H]-MPP$^+$ (ART 0150) were obtained from Revvity and American Radiolabeled Chemicals Inc. (ARC), respectively. Paroxetine (cat. no. AB 439408)

was obtained as its hydrochloride form from abcr GmbH (Karlsruhe, Germany). GBR12909 (as dihydrochloride) (cat. no. D052), *S*-(+)-AMPH (as its hemisulfate salt) (cat. no. A-5880), *p*CA (cat. no. C9635) as well as MON (as sodium salt) (cat. no. M5273) were received from Sigma-Aldrich (St. Louis, MO, USA). Ultima Gold™ XR (cat. no. 6013117) scintillation cocktail was provided by PerkinElmer (Waltham, USA) and used for 96-well-based assays. Rotiszint®Routine (1P1A.2) scintillation cocktail was obtained from Carl Roth (Karlsruhe, Germany) and used for release assays.

## 2.2 Cell culture

HEK-293 cells that stably express the human isoforms of SERT (= hSERT), DAT (= hDAT), and NET (= hNET) were used. Additionally, hSERT and hDAT were N-terminally tagged with YFP, whereas hNET was untagged. These stable cell lines were kindly provided (115). Cells were cultured in Dulbecco′s Modified Eagle′s Medium (DMEM) (cat. no. L0102) from Biowest (Bradenton, USA), which was supplemented with 10% fetal bovine serum (FBS) (cat. no. FBS-11A) from Capricorn Scientific GmbH (Ebsdorfergrund, Germany). Once the cells reached a density of approximately 80%, they were passaged to maintain a sub-confluent state or to prepare them for seeding in experimental plates (115). This was done by washing with 4-5 mL phosphate-buffered saline (PBS; 137 mM NaCl, 4.3 mM $Na_2HPO_4 \cdot 2\,H_2O$, 2.7 mM KCl, and 1.5 mM $KH_2PO_4$, adjusted with NaOH to pH 7.3). Afterwards, 1 mL of pre-warmed trypsin-EDTA solution (cat. no. T3924) was added to detach the cells. After 1 min, trypsinization was stopped by adding 9 mL of pre-warmed DMEM. The cells were then triturated to obtain a single-cell suspension (115). To ensure stable expression of MATs in HEK-293 cells, selection was maintained by adding 50 µg/mL Geneticin (G418) (cat. no. G418-B) from Capricorn Scientific GmbH (Ebsdorfergrund, Germany). Before seeding, 96-well plates were coated with poly-D-lysine (PDL) (as its hydrobromide form) (cat. no. P1149) from Sigma-Aldrich (St. Louis, MO, USA) the day before the experiments to prevent cell detachment during washing steps (114). For uptake inhibition assays, cells were seeded at a density of 38,000 cells/well into PDL-coated white, clear flat-bottom 96-well plates (cat. no. CLS3903) from Corning® (Kennebunk, USA) one day prior to the experiments. For release assays, cells were seeded into PDL-coated ibidi µ-slides VI $^{0.4}$ (cat. no. 80606; Gräfelfing, Germany) at a density of 90,000 cells/channel.

## 2.3 *In vitro* uptake inhibition assay

Experiments were performed as previously described (115), with minor modifications. 100% uptake was determined in wells without addition of the SOI. To determine nonspecific substrate

uptake via other mechanisms, blank wells contained a full uptake inhibitor at a concentration that completely inhibited transporter activity. For SERT, this was 30 µM paroxetine, and for DAT and NET, 50 µM GBR12909. The signals measured from these wells were considered the baseline signal of the assay. On the day of the experiment, two seven-point logarithmic or half-logarithmic dilution series of the SOI were prepared. The first dilution series was used for pre-incubation and included only the SOI at the desired concentration in Krebs-HEPES buffer (KHB). KHB contained 10 mM HEPES (Sigma H-3375), 120 mM NaCl (Sigma S-9625), 20 mM D-(+)-glucose monohydrate (cat. no. 49159) from Sigma-Aldrich (St. Louis, MO, USA), 3 mM KCl (Merck 1.04936.500), 2 mM $CaCl_2 \cdot 2H_2O$ (Merck 2382.1000), and 2 mM $MgCl_2 \cdot 6H_2O$ (Merck 5833.250). The buffer was adjusted to pH 7.3. This step allowed the compound to bind to the transporter prior to substrate addition (114). The second dilution series was the uptake solution, which contained the same concentration of SOI as in the pre-incubation solution, plus the tritiated substrate and was brought to the final volume with KHB. The substrate for SERT was 0.1 µM [$^3$H]-5-HT, for DAT 0.05 µM [$^3$H]-MPP$^+$, and for NET 0.015 µM [$^3$H]-MPP$^+$. DMEM was aspirated from the 96-well plate, and 200 µL of room-temperature KHB was added to each well. Each well was first treated with 50 µL of pre-incubation solution for 5 min. The wells were aspirated and refilled with 50 µL of uptake inhibition solution. The uptake time was 1 min for SERT and 3 min for DAT and NET (see Figure 7 for an overview).

| Transporter | Pre-incubation time [min] | Uptake time [min] | Blocker |
|---|---|---|---|
| SERT | 5 | 1 | 30 µM paroxetine |
| DAT | 5 | 3 | 50 µM GBR 12909 |
| NET | 5 | 3 | 50 µM GBR 12909 |

*Figure 5: Pre-incubation time, uptake time and the blockers used for the uptake inhibition assay.*

The uptake inhibition solution was aspirated, and wells were washed with ice-cold KHB. After aspiration, each well was subsequently filled with 200 µL of scintillation cocktail (Ultima Gold$^{TM}$ XR). The plate was counted in a liquid scintillation counter (Wallac MicroBeta Trilux 1450-021). The value measured in the negative control was subtracted from the measured uptake values at each SOI concentration to obtain the specific uptake. Uptake in the presence of the SOI was then expressed as a percentage of a positive control (100%), which contained only the substrate without any potentially transporter-inhibiting substance. From these measured uptake values, the half-maximal concentration ($IC_{50}$) was determined (115). The $IC_{50}$ value was determined by fitting a nonlinear regression curve using GraphPad Prism 8.0.1 (GraphPad Software Inc., San Diego, USA). The data were best described by a sigmoidal

dose-response model. Data were pooled from three independent experiments, each performed in triplicate.

## 2.4 Release assay

Experiments were conducted based on the previously described protocol (119,120), with slight modifications. This experiment was designed to test the benzofuran compounds for their release properties. Channels were pre-coated with PDL prior to seeding. 100 µL of HEK-293 cells expressing the required MAT ($0.9 \cdot 10^6$ cells/mL) were seeded into each channel of the ibidi µ-slides VI $^{0.4}$ (cat. no. 80606; Gräfelfing, Germany) and incubated overnight. On the day of the experiment, the substance solutions were prepared. Each solution was measured in triplicate per experiment, with three channels superfused with the same solution (SOI ± MON or positive control ± MON). The experiment was repeated three times. Each channel was first perfused with water for 15 min, followed by at least 5 min of KHB perfusion before insertion of the ibidi chambers containing the cells. For pre-incubation, cells were loaded with tritiated substrates: 50 µL of 0.05 µM [$^3$H]MPP$^+$ (used for DAT), 50 µL of 0.015 µM [$^3$H]MPP$^+$ (used for NET), and 50 µL of 0.1 µM [$^3$H]-5-HT (used for SERT). This loading phase was carried out for 20 min at 37 °C. Each vial was filled with 2 mL of scintillation cocktail Rotiszint®Routine (1P1A.2). Superfusion experiments were performed at concentrations around the $IC_{50}$ of the respective substance. Channels were superfused with SOI or positive control, both with or without MON, in KHB. The positive control consisted of 10 µM *S*-AMPH for DAT and NET, and 10 µM *p*CA for SERT. After the 20-min loading period, all channels were washed with 70 µL of room-temperature KHB. Afterwards, 90 µL were removed from each channel, and each channel was filled with 190 µL of room-temperature KHB. Superfusion was performed at a flow rate of approximately 0.5 mL/min and a targeted temperature of 21-23 °C. After insertion of the chambers into the superfusion apparatus, the system was perfused with KHB for 10 min to remove residual radiolabeled substrate and to establish a stable baseline. The experiment was then started, and fractions were collected every 2 min. From 0-6 min (3 fractions), channels were superfused with KHB to determine basal efflux, which served as the baseline. Subsequently, channels were superfused with KHB ± 10 µM MON for 8 min (4 fractions). Afterwards, all channels were superfused with their respective SOI ± MON or positive control ± MON for 10 min (5 fractions). Finally, each channel was superfused with 1% SDS solution for 6 min (3 fractions) to lyse the cells. Vials were then shaken and measured in a β-counter (Tri-Carb 2810 TR; PerkinElmer). The release in individual fractions was expressed as fractional release. First, the total radioactivity was determined by

summing all collected fractions, including those obtained by solubilization. Then, the radioactivity released in each 2-minute fraction was calculated as the percentage of the [$^3$H]-substrate still present in the cells (= total radioactivity – radioactivity released up to that point) during the 2-min collection interval. For the calculation, Excel (Microsoft) and GraphPad Prism 8.0.1 (GraphPad Software Inc., San Diego, USA) were used. Expressed as a formula (117):

$$fractional\ release\ [\%] = \frac{cpm\ (2\ \mathrm{min}\ fraction)}{total\ radioactivity - \sum previously\ released\ radioactivity} \cdot 100$$

Mean ± SD were calculated from the number of experiments. Statistical significance between KHB and MON conditions at the indicated time points was assessed using a mixed-effects model with Šidák correction for multiple comparisons. Differences were considered statistically significant at $p < 0.05$.

Concentration-response curves of the SOIs were determined by applying concentrations of $0.03 \cdot IC_{50}$, $0.1 \cdot IC_{50}$, $0.3 \cdot IC_{50}$, $1 \cdot IC_{50}$, and $3 \cdot IC_{50}$. For each concentration, at least three independent experiments ($n \geq 3$) were performed, with measurements performed in triplicate. The experiment was performed as described in Chapter 2.4 (Release Assay), except that the pretreatment phase (4·2 min ± MON) was omitted because MON was not used. Therefore, the experiment was carried out as follows: 3·2 min KHB pre-wash phase, 5·2 min SOI phase and 3·2 min 1% SDS phase. The calculations were performed in the same manner as described in Chapter 2.4. For generating the concentration-response curve, efflux was calculated after the fractional release values were obtained. This efflux was defined by averaging the release values of the SOI fractions once the release had stabilized, followed by subtracting the mean baseline value, yielding the release induced by the substance. Since each experiment was conducted in triplicate (three channels), the mean of these three channels was used for further analysis. Subsequently, the respective release values (y-axis) were plotted against their concentrations (x-axis) to determine the $EC_{50}$. The $EC_{50}$ value was determined by fitting a nonlinear regression curve. The data were best described by a sigmoidal dose-response model.

# 3 Results

## 3.1 Uptake inhibition assay

First, the $IC_{50}$ values of the compounds were determined using an uptake inhibition assay in MAT-expressing cell lines. The results showed that the compounds in the *S*-configuration displayed significantly lower $IC_{50}$ values at SERT compared with their *R*-configured enantiomers. The potency of uptake inhibition varied by approximately 6-fold (4.4 µM (*S*-βK-5-MABB) to 27.4 µM (*R*-βK-5-MABB)) up to 16.5-fold (6.3 µM (*S*-βK-6-MAPB) to 104.0 µM (*R*-βK-6-MAPB)). Moreover, the data indicated that the position of the substituent on the benzofuran ring affected uptake inhibition at SERT. Benzofurans with the substituent in position 6 were approximately 2 (7.7 µM (*S*-βK-6-MABB) to 4.4 µM *S*-βK-5-MABB)) to 3-fold (77.8 µM (*S*-βK-6-MABB) to 27.4 µM (*S*-βK-5-MABB)) less potent than those with the substituent in position 5. In contrast, the length of the alkyl side chain had only a minor impact on SERT inhibition, as the $IC_{50}$ values did not differ substantially (7.7 µM (*S*-βK-6-MABB) to 6.3 µM (*S*-βK-6-MAPB).

With respect to DAT, the *S*-configured compounds also exhibited approximately 5-fold (0.115 µM (*S*-βK-6-MABB) to 0.024 µM (*R*-βK-6-MABB)) to 6-fold (0.123 µM (*S*-βK-5-MABB) to 0.708 µM (*R*-βK-5-MABB)) greater potency compared with the *R*-configured isomers. The position of the substituent on the benzofuran ring had a similar impact on potency. When the substituent was located at position 6, the compound was about 5-fold (0.024 µM (*S*-βK-6-MABB) to 0.123 µM (*S*-βK-5-MABB)) to 6-fold (0.115 µM (*R*-βK-6-MABB) to 0.708 µM (*R*-βK-5-MABB)) more potent at DAT than when the substituent was in position 5. The length of the alkyl side chain influenced potency by approximately twofold (0.024 µM (*S*-βK-6-MABB) to 0.042 µM (*S*-βK-6-MAPB) and 0.115 µM (*R*-βK-6-MABB) to 0.234 µM ((*R*-βK-6-MAPB)).

For NET, stereochemistry plays a major role in determining potency, as observed for both SERT and DAT. The *S*-configured compounds exhibited approximately 1.5 (0.498 µM (*S*-βK-5-MABB) to 0.767 µM (*R*-βK-5-MABB)) to 6-fold (0.064 µM (*S*-βK-6-MABB) to 0.368 µM (*R*-βK-6-MABB)) greater potency at NET compared with the *R*-configured form. The position of the substituent also had a pronounced impact on potency. When the substituent was located at position 6, potency was a 2-fold (0.368 µM (*R*-βK-6-MABB) to 0.767 µM (*R*-βK-5-MABB)) to 8-fold (0.064 µM (*S*-βK-6-MABB) to 0.498 µM (*S*-βK-5-MABB)) higher compared with position 5. The length of the alkyl side chain influenced potency, with the 2-aminobutyl analogues being approximately 2-fold

(0.368 µM (*R*-βK-6-MABB) to 0.750 µM (*R*-βK-6-MAPB)) to 3-fold (0.064 µM((*S*-βK-6-MABB) to 0.205 µM (*S*-βK-6-MAPB)) more potent than their 2-aminopropyl counterparts.

All raw data are presented in the table below (Figure 9), which further illustrates that all tested compounds showed the strongest inhibitory effect on substrate uptake at DAT, followed by NET, while inhibition at SERT showed the lowest potency (an example: (*R*-βK-6-MABB): $IC_{50}$ (SERT) = 77.8 µM, $IC_{50}$ (DAT) = 0.115 µM and $IC_{50}$ (NET) = 0.368 µM).

To assess whether each compound acts as a releaser, a superfusion release assay was performed for each substance at the respective $IC_{50}$. An exception was made for *R*-βK-6-MABB and *R*-βK-6-MAPB, as their $IC_{50}$ values were very high, which would require an excessive amount of compound for the superfusion release assay at the $IC_{50}$ concentration. Therefore, for these compounds, the superfusion release assay was conducted at a concentration of 30 µM.

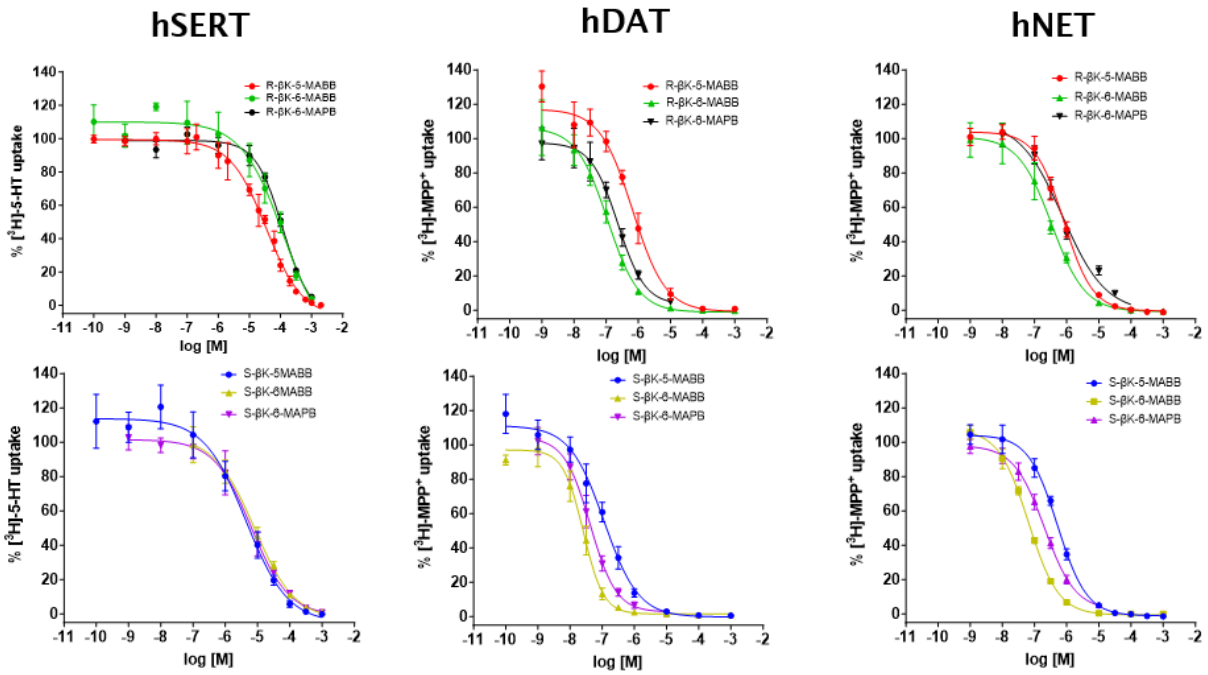


*Figure 6: Representation of the uptake inhibition curves. The x-axis shows the molar concentration of the tested compounds and the y-axis indicates the percentage uptake of the radiolabeled substrate. Above the graphs, the corresponding MAT to which both curves correspond is indicated. The data points are the mean ± standard deviation (SD) from three indipendent experiments, each performed in triplicate. To determine the half-maximal inhibitory concentration (IC50), the experimental data were plotted and fitted using non-linear regression with a sigmoidal dose-response curve.*

| Substance | Structure | SERT [µM] ± SD | DAT [µM] ± SD | NET [µM] ± SD |
|---|---|---|---|---|
| *S*-βK-5-MABB | 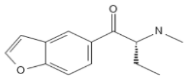 | 4.4 ± 1.5 | 0.123 ± 0.025 | 0.498 ± 0.078 |
| *R*-βK-5-MABB | 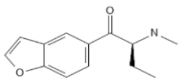 | 27.4 ± 2.6 | 0.708 ± 0.021 | 0.767 ± 0.112 |
| *S*-βK-6-MABB | 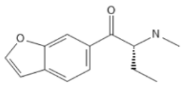 | 7.7 ± 0.6 | 0.024 ± 0.002 | 0.064 ± 0.006 |
| *R*-βK-6-MABB | 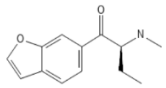 | 77.8 ± 6.7 | 0.115 ± 0.021 | 0.368 ± 0.062 |
| *S*-βK-6-MAPB | 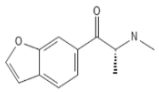 | 6.3 ± 2.7 | 0.042 ± 0.001 | 0.205 ± 0.035 |
| *R*-βK-6-MAPB | 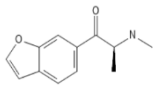 | 104.0 ± 13.3 | 0.234 ± 0.034 | 0.750 ± 0.112 |

*Figure 7: Overview of the results from the uptake inhibition assays. The graph shows the tested compounds, including their chemical structures and $IC_{50}$ values for the respective MATs.*

## 3.2 Screening for releasing activity

During the superfusion release assay, the concentrations used to determine the release properties of the compounds slightly deviated from the experimentally determined $IC_{50}$ values (e.g., *R*-βK-5-MABB was tested at 29 µM instead of 27.4 µM and *S*-βK-6-MAPB at 6.5 µM instead of 6.3 µM). All tested compounds exhibited release at SERT, which was further enhanced by MON. The release of the compounds in the *S*-configuration was higher than that of the *R*-configuration. Moreover, the MON-induced enhancement of release was overall stronger for the *S*-configured compounds compared to the *R*-configured compounds.

At DAT, release occurred only for *R*-βK-6-MAPB, which was significantly enhanced by MON. For NET, release occurred for both *R*-βK-6-MAPB and *S*-βK-6-MAPB. The *R*-configured compound produced a higher percentage of release than the *S*-configured compound. Furthermore, the effect of MON at NET was not statistically significant. The observed difference between MON and non-MON conditions has also been reported otherwise (56).

Since all compounds induced substantial release at SERT, they were considered releasers. However, due to the very high $IC_{50}$ values of the *R*-configured compounds, concentration-response curves were not generated for these substances, but only for the *S*-configured compounds. At DAT, *R*-βK-6-MAPB produced a pronounced increase in release. Additionally, the effect of MON was statistically significant, so this compound was also classified as a releaser. At NET, although the effect of MON was not statistically significant, the release for both compounds was sufficiently large to warrant the determination of a concentration-response curve.

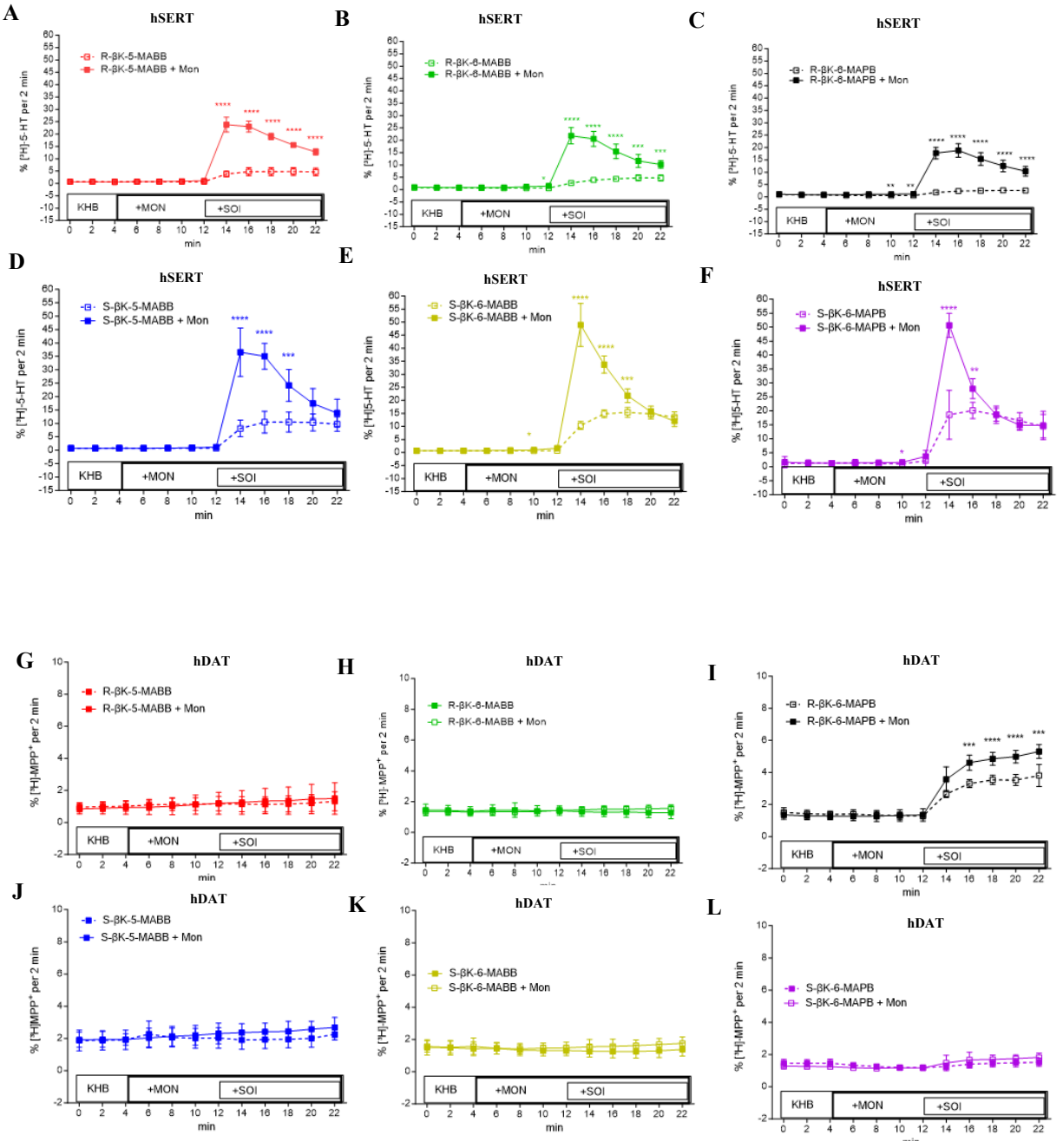


(Figure continued on next page)

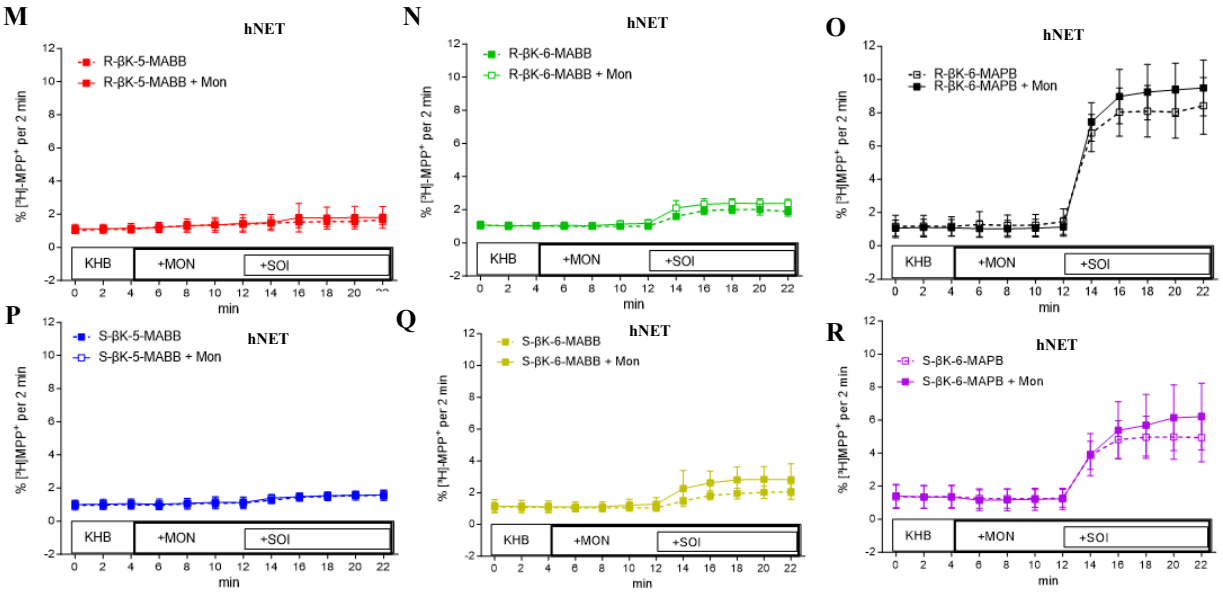


*Figure 8: Release of preloaded [$^3$H]-5-HT or [$^3$H]-MPP$^+$ in HEK-293 cells via stably expressing SERT, DAT or NET: Each graph shows the release profile of [$^3$H]-5-HT at SERT (A-F), of [$^3$H]-MPP$^+$at DAT (G-L) or NET (M-R) of a compound with and without MON in the superfusion release assay. The x-axis represents the time elapsed since the start of the experiment, and the y-axis displays the percentage of radiolabeled substrate released every two minutes. Compounds were applied between 14 and 24 min at concentrations near their respective $IC_{50}$ values either in KHB (dashed line) or in the presence of 10 µM MON in KHB (solid line). Values represent the mean ± SD of 3 independent cell culture preparations (n = 3), performed in triplicate. Statistical significance between KHB and MON conditions at the indicated time points was assessed using a mixed-effects model with Šidák correction for multiple comparisons, confirming the releasing activity of the tested compounds. Control experiments included the known full releaser pCA for SERT and S-AMPH for DAT and NET. Differences were considered statistically significant at $p < 0.05$. Symbols indicate significance levels as follows: *$p < 0.05$, **$p < 0.01$, ***$p < 0.001$ and ****$p < 0.0001$.*

| Summary of Tested Substances and Their Releasing Properties in Superfusion | | | | |
|---|---|---|---|---|
| **Substance** | **Structure** | **SERT** | **DAT** | **NET** |
| *S*-βK-5-MABB | 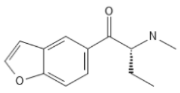 | Yes | No | No |
| *R*-βK-5-MABB | 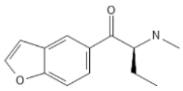 | Yes | No | No |
| *S*-βK-6-MABB | 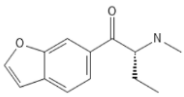 | Yes | No | No |
| *R*-βK-6-MABB | 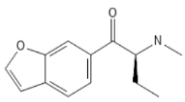 | Yes | No | No |
| *S*-βK-6-MAPB | 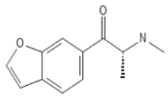 | Yes | No | Yes |
| *R*-βK-6-MAPB | 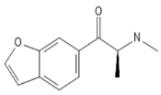 | Yes | Yes | Yes |

*Figure 9: Overview of the results from the superfusion release assays. The table shows the tested compounds, including their structural formulas, and indicates whether they elicit a release effect at each MAT, allowing classification as releasers.*

## 3.3 Concentration-response analysis of releasing compounds

At SERT, all three compounds exhibited similar $EC_{50}$ values ($EC_{50}$(*S*-βK-5-MABB) = 1.07 µM, $EC_{50}$(*S*-βK-6-MABB) = 1.95 µM and $EC_{50}$(*S*-βK-5-MAPB) = 1.13 µM). Regarding maximal release ($E_{max}$), *S*-βK-6-MAPB induced approximately twice the release of *S*-βK-5-MABB ($E_{max}$(*S*-βK-6-MAPB) = 15.25 % to $E_{max}$(*S*-βK-5-MABB) = 7.36 %) and about 1.2-fold the release of *S*-βK-6-MABB ($E_{max}$(*S*-βK-6-MAPB) = 15.25 % to $E_{max}$(*S*-βK-6-MABB) =12.61 %). These values were normalized to *p*CA, indicating that *S*-βK-5-MABB corresponded to approximately 41.6 %, *S*-βK-6-MABB approximately 71.2 %, and *S*-βK-6-MAPB approximately 86.1 % of *p*CA's release (Emax(*p*CA) = 17.71 %).

At DAT, *R*-βK-6-MAPB had an $EC_{50}$ of 0.105 µM and an $E_{max}$ of 3.13 %. Compared to *S*-AMPH, *R*-βK-6-MAPB produced approximately 33.1 % of *S*-AMPH's release.

At NET, *S*-βK-6-MAPB and *R*-βK-6-MAPB both exhibited nearly identical $EC_{50}$ values ($EC_{50}$(*S*-βK-6-MAPB) = 0.115 µM and $EC_{50}$(*R*-βK-6-MAPB) = 0.113 µM). In terms of $E_{max}$, *R*-βK-6-MAPB induced 1.3-fold higher maximal release than *S*-βK-6-MAPB ($E_{max}$(*R*-βK-6-MAPB) = 7.88 % to $E_{max}$(*S*-βK-6-MAPB) = 6.01 %). When compared to *S*-AMPH, *S*-βK-6-MAPB showed similar maximal release to *S*-AMPH, whereas *R*-βK-6-MAPB exhibited 1.3-fold higher maximal release than *S*-AMPH ($E_{max}$ (*S*-AMPH) = 6.05 %).

*R*-βK-6-MAPB induced release at all three MATs, with NET showing approximately 2.5-fold higher release ($E_{max}$ (*R*-βK-6-MAPB, NET) = 7.88 % to $E_{max}$ (*S*-βK-6-MAPB, DAT) = 3.13 %). *S*-βK-6-MAPB produced release at both SERT and NET, with the effect at SERT being about 2.5-fold stronger ($E_{max}$ (*S*-βK-6-MAPB, SERT) = 15.25 % to $E_{max}$ (*S*-βK-6-MAPB, NET) = 6.01 %). In contrast, *S*-βK-5-MABB and *S*-βK-6-MABB both elicited release exclusively at SERT.

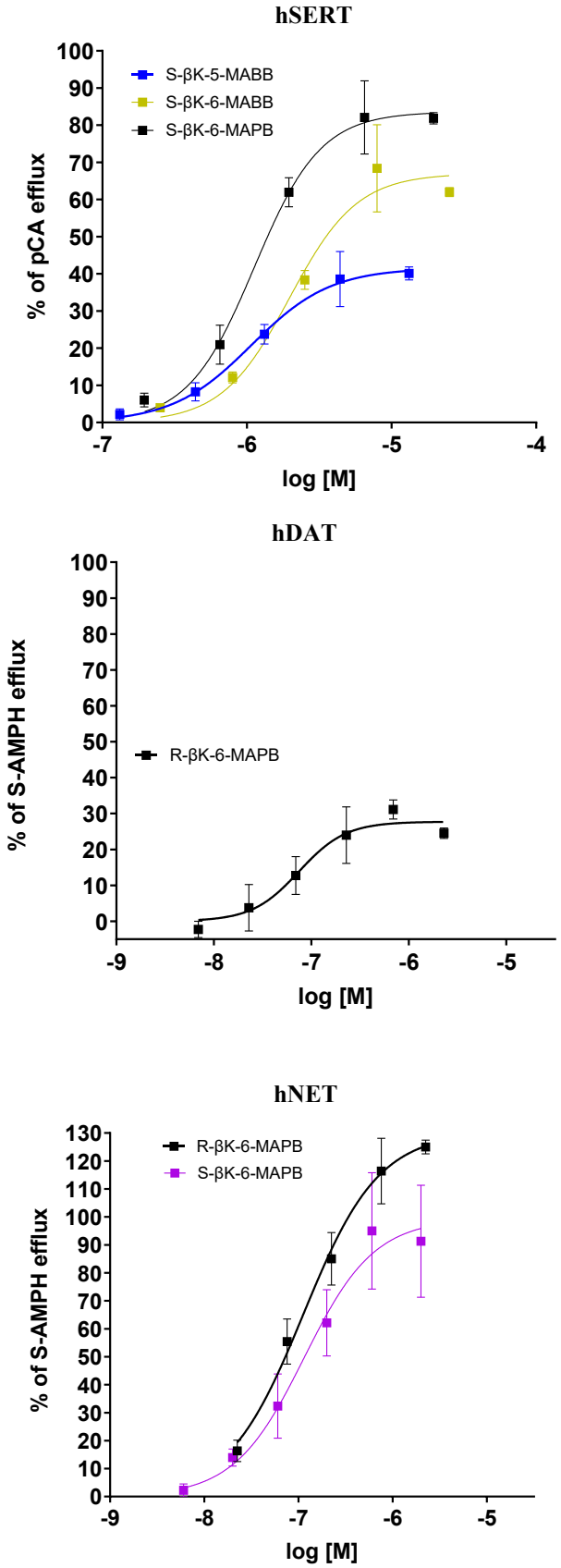


*Figure 10: Release of preloaded [$^3$H]-substrate in HEK-293 cells stably expressing MAT. Each graph shows the release profile of [$^3$H]-substrate for a single compound in the superfusion release assay at one MAT. The x-axis represents the logarithmic molar concentration of the compound, while the y-axis displays the percentage of radiolabeled substrate released relative to the control substance. Values represent the mean ± SD of three*

*independent cell culture preparations (n = 3), each performed in triplicate. Control experiments included the known full releaser for the respective MAT.*

| MAT | **Substance** | **Structure** | **EC50 (95 % CI) [µM]** | **Emax (95 % CI) [%]** | **% (of full releaser)** |
|---|---|---|---|---|---|
| SERT | *S*-βK-5-MABB | 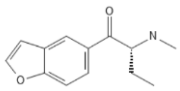 | **1.071** (0.784 – 1.463) | **7.36** (6.49 – 8.24) | 41.6 |
| SERT | *S*-βK-6-MABB | 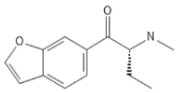 | **1.947** (1.444 – 2.625) | **12.61** (11.09 – 14.13) | 71.2 |
| SERT | *S*-βK-6-MAPB | 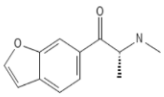 | **1.127** (0.924 – 1.373) | **15.25** (14.24 – 16.26) | 86.1 |
| DAT | *R*-βK-6-MAPB | 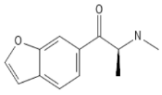 | **0.105** (0.043 – 0.260) | **3.13** (1.91 – 4.34) | 33.1 |
| NET | *R*-βK-6-MAPB | 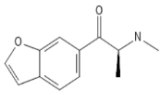 | **0.113** (0.079 – 0.160) | **7.88** (7.02 – 8.74) | 130.2 |
| NET | *S*-βK-6-MAPB | 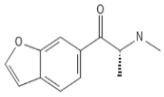 | **0.115** (0.065 – 0.204) | **6.01** (4.81 – 7.21) | 99.3 |

*Figure 11: Concentration-response curve results from the superfusion release assay, showing each tested compound with its corresponding transporter, potency ($EC_{50}$), efficacy ($E_{max}$) and release percentage relative to a standard full releaser (pCA for SERT and S-AMPH for DAT and NET).*

# 4 Discussion

Amphetamines play an important role in neuropsychopharmacology and have both therapeutic and abuse-related properties. Recent phase 3 studies indicate increasing interest in MDMA, which could serve as a therapeutic agent in the treatment of PTSD (107,108) and have led to granting market access for MDMA in Australia (121) and off-label use in Switzerland (122,123). One goal of current research efforts in the pharmacotherapeutic treatment of PTSD is to develop MDMA derivatives that exhibit improved pharmacological characteristics, such as an enhanced safety profile and potentially higher therapeutic efficacy (56). In this context, benzofuran derivatives may represent promising therapeutic agents. The therapeutic effect of MDMA is thought to primarily rely on transporter-mediated release of serotonin (124), although additional mechanisms such as oxytocin (64) may contribute. A disadvantage of amphetamines is their noradrenergic activity, which can influence the cardiovascular system and may lead to increased contractile force, elevated heart rate, and cardiovascular strain (125). A reduced effect on the noradrenergic system may therefore mitigate these cardiotoxic effects and may be associated with an improved safety profile. Since the addictive effects of psychostimulants are associated with the dopaminergic system (9), reduced transporter-mediated release or influence on the dopaminergic system via DAT may reduce dopaminergic reinforcement mechanisms associated with abuse liability. Therefore, release at DAT and NET may be undesirable for the use of benzofurans as alternatives to MDMA, whereas release at SERT may prove to be beneficial.

A suitable comparison to existing data is provided by a previous master's thesis conducted in the Sitte laboratory, which analysed both stereoisomers of βK-5-MAPB (126). Although these data are not peer-reviewed, they have the advantage that the experiments were conducted in the same laboratory under identical experimental conditions, allowing better comparability. Data for MDMA are available under similar experimental conditions, reporting $IC_{50}$ values and release profiles at MATs (56).

Regarding uptake inhibition, the present findings are consistent with previous observations showing that benzofuran cathinones exhibit the highest inhibitory potency at DAT, followed by NET, and SERT (126). Compared with MDMA (56), the benzofuran cathinones tested in the current study exhibited stronger inhibitory potency at all three MATs (see Figure 7), suggesting that structural modifications, including the β-keto group and benzofuran ring system, may contribute to enhanced transporter inhibition. These findings further allow an assessment of the structural determinants of MAT inhibition.

Among the investigated structural features, stereochemistry had the strongest and most consistent influence on inhibitory potency across SERT, DAT, and NET. The *S*-enantiomer exhibited higher potency than the *R*-enantiomer, suggesting a stereoselective interaction with the binding sites of the transporters. This is consistent with previous findings (124,126), although the *R*-enantiomer was reported to be more potent at DAT than the *S*-enantiomer (124). Despite being performed in different experimental systems (HEK-293 cells vs. rat brain synaptosomes), these studies demonstrated a substantial difference in potency between stereoisomers. Taken together, these findings suggest that the *R*-enantiomers contribute less strongly to transporter inhibition.

The position of the substituent on the benzofuran ring further modulates uptake inhibition. At SERT, substitution at position 6 moderately reduced inhibition, while at DAT and NET substitution at position 6 enhanced potency. This observation aligns with previous findings (41,124,127). However, one study reported slightly higher potency at NET for substitution in position 6 (41). These findings further support the hypothesis (41) that an oxygen atom in the para position relative to the aminoalkyl side chain enhances serotonergic properties while reducing dopaminergic ones.

The length of the alkyl chain also influences the potency of the compound: βK-6-MABB, which contains a butyl chain, exhibited stronger inhibition than its corresponding propyl analogue βK-6-MAPB across all tested transporters, except for the *S*-enantiomer at SERT. This deviation from the general trend may be due to the high variability of the data, as reflected by overlapping standard deviations. A previous study reported increased potency at SERT and DAT for the butyl analogues but observed the opposite effect at NET (42). However, these discrepancies should be interpreted with caution and may arise from differences in steric and conformational properties of the respective ring systems, which could influence how the alkyl side chains interact with the transporter binding site.

Taken together, these findings indicate that the stereochemistry of the compounds strongly influences inhibitory potency at all three MATs, with the *S*-form representing the more potent enantiomer. In addition, both the position of the substituent on the benzofuran ring and the length of the alkyl chain affect inhibitory activity. Para-substitution appears to enhance serotonergic effects while reducing dopaminergic effects, and the butyl chain generally confers stronger inhibition than the propyl chain. These effects are particularly relevant for compounds with steep concentration-response curves, where inhibition increases sharply within a narrow concentration range, as observed for the tested compounds.

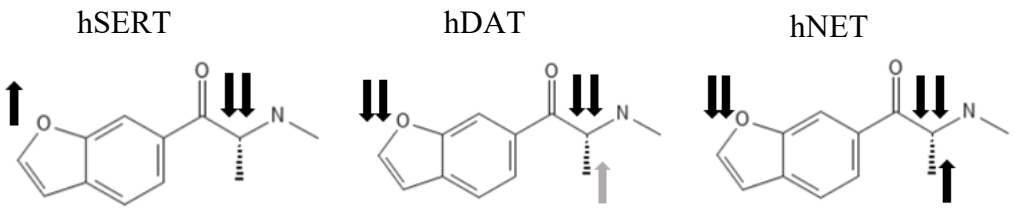


*Figure 12: Uptake inhibition effects of benzofuran cathinones at MATs. An upward arrow indicates an increase in $IC_{50}$, whereas a downward arrow indicates a decrease. The number of arrows reflects the magnitude of the effect: more arrows correspond to a stronger influence. The effect of stereochemistry is indicated above the chiral carbon. A gray arrow indicates an uncertain effect, while black arrows indicate more likely effects.*

Since uptake inhibition assays do not distinguish between transporter substrates and non-transported competitive inhibitors (116,117), the superfusion release assay was necessary to further characterize releaser properties.

With respect to releasing properties, the data indicated that all tested substances acted as releasers at SERT, as all compounds showed a significant enhancement in the presence of MON. At DAT and NET, only compounds with a propyl chain showed release, whereas the remaining compounds showed no detectable effect. The release at DAT was restricted to the *R*-enantiomer of the propyl form. At NET, the propyl derivatives showed release, but MON did not significantly enhance this effect. Nevertheless, because the increase in release was pronounced and the substrate $MPP^+$ cannot passively diffuse into the cell due to its charge (128), the observed effect strongly suggests transporter-mediated release rather than uptake inhibition. The literature presents inconsistent findings regarding transporter-specific release. Studies conducted in rat brain synaptosomes (124,129) as well as in HEK-293 cells (126,127) do not show a uniform pattern across transporters. However, unlike MDMA (56), which induces release at SERT, DAT, and NET, *S*-βK-5-MABB and *S*-βK-6-MABB only showed release at SERT, suggesting a more selective release profile. The release data further allow an assessment of how structural modifications influence transporter-mediated monoamine release.

At SERT, stereochemistry appears to strongly influence release properties, as the *S*-form produced stronger release than the *R*-form at the $IC_{50}$, both in the presence and absence of MON. This is consistent with findings from the previous master thesis mentioned before (126). This interpretation assumes that the release of the *R*-form does not increase disproportionately at concentrations outside the $IC_{50}$ range. All three tested *S*-enantiomers exhibited $EC_{50}$ values between 1-2 µM, indicating that they act within a very similar concentration range and are therefore similarly potent in inducing efflux. Similar $EC_{50}$ values for benzofurans were reported within a range of 0.2-3.9 µM (126). A key difference of the tested benzofurans, however, lies in their efficacy. The position of the substituent on the benzofuran ring seems to have a strong influence on efficacy, ranging from *S*-βK-5-MABB ($E_{max}$ = 7.4 %) to *S*-βK-6-MABB

($E_{max}$ = 12.6 %). In addition, the alkyl-chain length appears to influence efficacy, with the 2-aminopropyl group producing a stronger effect ($E_{max}$ = 15.3 %) than the 2-aminobutyl group ($E_{max}$ = 12.6 %). Compared with the full releaser *p*CA (17.7 %), *S*-βK-5-MABB exhibited only about 42 % of *p*CA's release, which may indicate partial releasing properties. For *S*-βK-6-MABB, this value was about 71 % *p*CA's release, indicating stronger releasing properties, whereas *S*-βK-6-MAPB reached 86 % *p*CA's release and appears to act as a full releaser. In summary, $EC_{50}$ values varied within a relatively narrow micromolar range, while $E_{max}$ values ranged from partial to near-full release. This suggests that structural differences primarily influence intrinsic efficacy rather than functional potency within the tested range. These findings are supported by mechanistic models of MATs, which show that partial releasers exhibit reduced maximal release efficacy compared with full releasers (130). Possible explanations for these observed variations in $E_{max}$ may arise from ligand-specific conformational dynamics of the transporter, as different ligands stabilize specific transporter states that could influence maximal release (131).

The concentration-response curve at DAT shows that *R*-βK-6-MAPB produced moderate release, with an $E_{max}$ of approximately 33 %, relative to *S*-AMPH. Therefore, it may be classified as a partial releaser. Such partial release effects at DAT have also been reported in the literature (132). One possible explanation is that different DAT ligands may stabilize distinct conformational states of the transporter (133). Consistent with these findings, DAT-mediated release was observed only for the R-enantiomer of the benzofuran cathinone, whereas different results were reported for the corresponding amphetamine analogue (126).

At NET, the data showed that the length of the alkyl chain was a key determinant of release, as only the 2-aminopropyl group produced release, whereas no release was observed for the 2-aminobutyl group. The available literature reports varying findings regarding NET release. While some studies report NET release for propyl derivatives (126,127,129), another study observed release also with butyl-substituted compounds (124). It should be noted, however, that the latter study used a different experimental system (rat brain synaptosomes) and only tested amphetamine analogues, which could explain the discrepancy. Another observation is that the *R*-enantiomer (7.9 %) produced a stronger release effect than the *S*-enantiomer (6.0 %), even though the 95 % confidence intervals slightly overlapped (*R*-βK-6-MAPB = 7.88 % (7.02 % - 8.74 %) and *S*-βK-6-MAPB = 6.01 % (4.81 % - 7.21 %)). This finding is consistent with the literature (126). However, it contrasts with results obtained for the amphetamine derivatives. Consistent with these observations, another study (124) also reported that the *R*-enantiomers induced lower maximal release.

*R*-βK-6-MAPB acts as a full releaser at NET but only as a partial releaser at DAT. Such transporter-specific differences have also been reported for mephedrone (132). These differences may arise from dynamic, conformational, or structural differences between the transporters. Studies conducted in rat brain synaptosomes (124,129) as well as in HEK-293 cells (126,127) do not show a uniform pattern across the tested transporters. When considering all available data, a trend may possibly be observed, suggesting that SERT and NET tend to exhibit higher maximal release ($E_{max}$) compared to DAT. However, a study performed in rat synaptosomes (124) reported no significant differences between transporters, whereas a study in HEK-293 cells observed higher release at hDAT than at hSERT for a benzofuran cathinone analogue (126). Therefore, transporter-specific differences in $E_{max}$ appear to be context-dependent and influenced by the experimental system. In the present study, release at NET and DAT was also observed exclusively for propyl-substituted compounds, whereas butyl analogues failed to induce release at these transporters. This may indicate that alkyl chain length contributes to transporter selectivity in release assays. Furthermore, the corresponding amphetamine analogues exhibited stronger releasing properties overall (126). Taken together, the present findings indicate that structural modifications in benzofuran cathinones modulate transporter selectivity as well as maximal release efficacy in a context-dependent manner.

For the concentration-response experiments used to characterize release properties, temperature was checked and documented prior to each experiment to ensure valid measurements.

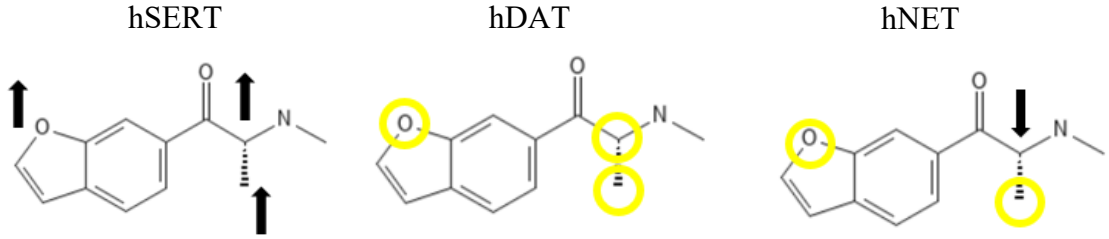


*Figure 13: Effects of structural features of benzofuran cathinones on their release efficacy ($E_{max}$) at MATs. The effect of stereochemistry is indicated above the chiral carbon atom. Yellow-circled areas highlight the key structural features necessary to elicit a release effect at MATs.*

# 5 Conclusion

Based on the previously discussed findings, *S*-βK-6-MAPB may be less suitable as an alternative substance for treating PTSD. In contrast, *S*-βK-5-MABB and *S*-βK-6-MABB demonstrate SERT-mediated release without significant release activity at DAT or NET, suggesting a more targeted and potentially safer pharmacological profile. Their strong uptake inhibition of radiolabeled substrates at DAT and NET, without inducing release, suggests direct transporter inhibition rather than substrate-mediated release. As transporter substrates are generally expected to induce release according to the alternating access model, the absence of release supports a sole inhibitory mechanism. The extent of SERT-mediated monoamine release required for therapeutic effects in PTSD has not yet been clearly established. For a more precise classification, investigations using patch-clamp techniques and *in vivo* examinations utilizing behavioral pharmacological experiments would be needed. Overall, these findings suggest that selective serotonergic release can be achieved through structural modifications in benzofuran cathinones. This may improve their pharmacological profile for the treatment of PTSD, provided that future toxicological studies confirm their safety.

# 6 References


1. Kristensen AS, Andersen J, Jørgensen TN, Sørensen L, Eriksen J, Loland CJ, et al. SLC6 Neurotransmitter Transporters: Structure, Function, and Regulation. Pharmacological Reviews. 2011 Sep 1;63(3):585–640. doi:10.1124/pr.108.000869

2. Sitte HH, Freissmuth M. Amphetamines, new psychoactive drugs and the monoamine transporter cycle. Trends Pharmacol Sci. 2015 Jan;36(1):41–50. doi:10.1016/j.tips.2014.11.006 PubMed PMID: 25542076; PubMed Central PMCID: PMC4502921.

3. Caveney S, Cladman W, Verellen L, Donly C. Ancestry of neuronal monoamine transporters in the Metazoa. J Exp Biol. 2006 Dec 15;209(24):4858–68. doi:10.1242/jeb.02607

4. Pickel VM, Chan J. Ultrastructural Localization of the Serotonin Transporter in Limbic and Motor Compartments of the Nucleus Accumbens. J Neurosci. 1999 Sep 1;19(17):7356–66. doi:10.1523/JNEUROSCI.19-17-07356.1999 PubMed PMID: 10460242; PubMed Central PMCID: PMC6782507.

5. Aggarwal S, Mortensen OV. Discovery and Development of Monoamine Transporter Ligands. Adv Neurobiol. 2023;30:101–29. doi:10.1007/978-3-031-21054-9_4 PubMed PMID: 36928847; PubMed Central PMCID: PMC10074400.

6. Hellsberg E, Boytsov D, Chen Q, Niello M, Freissmuth M, Rudnick G, et al. Identification of the potassium-binding site in serotonin transporter. Proc Natl Acad Sci U S A. 121(18):e2319384121. doi:10.1073/pnas.2319384121 PubMed PMID: 38652746; PubMed Central PMCID: PMC11067047.

7. Nikolaus S, Müller HW, Hautzel H. Different patterns of 5-HT receptor and transporter dysfunction in neuropsychiatric disorders--a comparative analysis of in vivo imaging findings. Rev Neurosci. 2016 Jan;27(1):27–59. doi:10.1515/revneuro-2015-0014 PubMed PMID: 26376220.

8. The dopamine transporter antiports potassium to increase the uptake of dopamine | Nature Communications [Internet]. [cited 2025 Sep 29]. Available from: https://www.nature.com/articles/s41467-022-30154-5

9. Chen R, Tilley MR, Wei H, Zhou F, Zhou FM, Ching S, et al. Abolished cocaine reward in mice with a cocaine-insensitive dopamine transporter. Proc Natl Acad Sci U S A. 2006 Jun 13;103(24):9333–8. doi:10.1073/pnas.0600905103 PubMed PMID: 16754872; PubMed Central PMCID: PMC1482610.

10. Tan J, Xiao Y, Kong F, Zhang X, Xu H, Zhu A, et al. Molecular basis of human noradrenaline transporter reuptake and inhibition. Nature. 2024 Aug;632(8026):921–9. doi:10.1038/s41586-024-07719-z

11. Bogdanski DF, Brodie BB. THE EFFECTS OF INORGANIC IONS ON THE STORAGE AND UPTAKE OF H3-NOREPINEPHRINE BY RAT HEART SLICES. The Journal of Pharmacology and Experimental Therapeutics. 1969 Feb 1;165(2):181–9. doi:10.1016/S0022-3565(25)28178-2

12. Berfield JL, Wang LC, Reith MEA. Which Form of Dopamine Is the Substrate for the Human Dopamine Transporter: the Cationic or the Uncharged Species? *. Journal of Biological Chemistry. 1999 Feb 19;274(8):4876–82. doi:10.1074/jbc.274.8.4876 PubMed PMID: 9988729.

13. Schicker K, Uzelac Z, Gesmonde J, Bulling S, Stockner T, Freissmuth M, et al. Unifying Concept of Serotonin Transporter-associated Currents *. Journal of Biological Chemistry. 2012 Jan 2;287(1):438–45. doi:10.1074/jbc.M111.304261 PubMed PMID: 22072712.

14. Bhat S, El-Kasaby A, Kasture A, Boytsov D, Reichelt JB, Hummel T, et al. A mechanism of uncompetitive inhibition of the serotonin transporter. Elife. 2023 Jan 17;12:e82641. doi:10.7554/eLife.82641 PubMed PMID: 36648438; PubMed Central PMCID: PMC9883013.

15. Hong WC, Amara SG. Membrane Cholesterol Modulates the Outward Facing Conformation of the Dopamine Transporter and Alters Cocaine Binding. J Biol Chem. 2010 Oct 15;285(42):32616–26. doi:10.1074/jbc.M110.150565 PubMed PMID: 20688912; PubMed Central PMCID: PMC2952264.

16. Morissette M, Morin N, Rouillard C, Di Paolo T. Membrane cholesterol removal and replenishment affect rat and monkey brain monoamine transporters. Neuropharmacology. 2018 May 1;133:289–306. doi:10.1016/j.neuropharm.2018.01.039

17. Zeppelin T, Ladefoged LK, Sinning S, Periole X, Schiøtt B. A direct interaction of cholesterol with the dopamine transporter prevents its out-to-inward transition. PLoS Comput Biol. 2018 Jan;14(1):e1005907. doi:10.1371/journal.pcbi.1005907 PubMed PMID: 29329285; PubMed Central PMCID: PMC5811071.

18. Scanlon SM, Williams DC, Schloss P. Membrane cholesterol modulates serotonin transporter activity. Biochemistry. 2001 Sep 4;40(35):10507–13. doi:10.1021/bi010730z PubMed PMID: 11523992.

19. Laursen L, Severinsen K, Kristensen KB, Periole X, Overby M, Müller HK, et al. Cholesterol binding to a conserved site modulates the conformation, pharmacology, and transport kinetics of the human serotonin transporter. J Biol Chem. 2018 Mar 9;293(10):3510–23. doi:10.1074/jbc.M117.809046 PubMed PMID: 29352106; PubMed Central PMCID: PMC5846164.

20. Rudin D, Luethi D, Niello M, Yang JW, Burger I, Sandtner W, et al. Cell membrane cholesterol affects serotonin transporter efflux due to altered transporter oligomerization. Mol Psychiatry. 2025 Sep 2;1–13. doi:10.1038/s41380-025-03201-y

21. Erickson JD, Eiden LE. Functional Identification and Molecular Cloning of a Human Brain Vesicle Monoamine Transporter. Journal of Neurochemistry. 1993;61(6):2314–7. doi:10.1111/j.1471-4159.1993.tb07476.x

22. Pothos EN, Davila V, Sulzer D. Presynaptic Recording of Quanta from Midbrain Dopamine Neurons and Modulation of the Quantal Size. J Neurosci. 1998 Jun 1;18(11):4106–18. doi:10.1523/JNEUROSCI.18-11-04106.1998 PubMed PMID: 9592091.

23. Alwindi M, Bizanti A. Vesicular monoamine transporter (VMAT) regional expression and roles in pathological conditions. Heliyon. 2023 Nov 1;9(11):e22413. doi:10.1016/j.heliyon.2023.e22413

24. Knoth J, Isaacs JM, Njus D. Amine transport in chromaffin granule ghosts. pH dependence implies cationic form is translocated. J Biol Chem. 1981;256(13):6541–3. doi:10.1016/s0021-9258(19)69022-8

25. Anne C, Gasnier B. Chapter Three - Vesicular Neurotransmitter Transporters: Mechanistic Aspects. In: Bevensee MO, editor. Current Topics in Membranes [Internet]. Academic Press; 2014 [cited 2025 Sep 28]. p. 149–74. (Exchangers). Available from: https://www.sciencedirect.com/science/article/pii/B9780128002230000037 doi:10.1016/B978-0-12-800223-0.00003-7

26. Guillot TS, Shepherd KR, Richardson JR, Wang MZ, Li Y, Emson PC, et al. Reduced vesicular storage of dopamine exacerbates methamphetamine-induced neurodegeneration and astrogliosis. J Neurochem. 2008 Sep;106(5):2205–17. doi:10.1111/j.1471-4159.2008.05568.x PubMed PMID: 18643795; PubMed Central PMCID: PMC4086661.

27. Biel JH, Bopp BA. Amphetamines: Structure-Activity Relationships. In: Iversen LL, Iversen SD, Snyder SH, editors. Stimulants [Internet]. Boston, MA: Springer US; 1978 [cited 2025 Sep 12]. p. 1–39. Available from: https://doi.org/10.1007/978-1-4757-0510-2_1 doi:10.1007/978-1-4757-0510-2_1

28. Sulzer D, Sonders MS, Poulsen NW, Galli A. Mechanisms of neurotransmitter release by amphetamines: A review. Progress in Neurobiology. 2005 Apr 1;75(6):406–33. doi:10.1016/j.pneurobio.2005.04.003

29. Sulzer D. How Addictive Drugs Disrupt Presynaptic Dopamine Neurotransmission. Neuron. 2011 Feb 24;69(4):628–49. doi:10.1016/j.neuron.2011.02.010 PubMed PMID: 21338876; PubMed Central PMCID: PMC3065181.

30. Han DD, Gu HH. Comparison of the monoamine transporters from human and mouse in their sensitivities to psychostimulant drugs. BMC Pharmacol. 2006 Mar 3;6:6. doi:10.1186/1471-2210-6-6 PubMed PMID: 16515684; PubMed Central PMCID: PMC1448202.

31. Rickli A, Hoener MC, Liechti ME. Monoamine transporter and receptor interaction profiles of novel psychoactive substances: Para-halogenated amphetamines and pyrovalerone cathinones. European Neuropsychopharmacology. 2015 Mar 1;25(3):365–76. doi:10.1016/j.euroneuro.2014.12.012

32. Sonders MS, Zhu SJ, Zahniser NR, Kavanaugh MP, Amara SG. Multiple Ionic Conductances of the Human Dopamine Transporter: The Actions of Dopamine and Psychostimulants. J Neurosci. 1997 Feb 1;17(3):960–74. doi:10.1523/JNEUROSCI.17-03-00960.1997 PubMed PMID: 8994051; PubMed Central PMCID: PMC6573182.

33. Peter D, Jimenez J, Liu Y, Kim J, Edwards RH. The chromaffin granule and synaptic vesicle amine transporters differ in substrate recognition and sensitivity to inhibitors. Journal of Biological Chemistry. 1994 Mar 11;269(10):7231–7. doi:10.1016/S0021-9258(17)37272-1

34. Blaschko H, Richter D, Schlossmann H. The inactivation of adrenaline. The Journal of Physiology. 1937 Jun 17;90(1):1–17. doi:10.1113/jphysiol.1937.sp003497

35. Mantle TJ, Tipton KF, Garrett NJ. Inhibition of monoamine oxidase by amphetamine and related compounds. Biochemical Pharmacology. 1976 Sep 15;25(18):2073–7. doi:10.1016/0006-2952(76)90432-9

36. Scorza MaC, Carrau C, Silveira R, Zapata-Torres G, Cassels BK, Reyes-Parada M. Monoamine Oxidase Inhibitory Properties of Some Methoxylated and Alkylthio Amphetamine Derivatives: Structure–Activity Relationships. Biochemical Pharmacology. 1997 Dec 15;54(12):1361–9. doi:10.1016/S0006-2952(97)00405-X

37. Khoshbouei H, Wang H, Lechleiter JD, Javitch JA, Galli A. Amphetamine-induced Dopamine Efflux: A VOLTAGE-SENSITIVE AND INTRACELLULAR Na+-DEPENDENT MECHANISM *. Journal of Biological Chemistry. 2003 Apr 4;278(14):12070–7. doi:10.1074/jbc.M212815200 PubMed PMID: 12556446.

38. Loder MK, Melikian HE. The dopamine transporter constitutively internalizes and recycles in a protein kinase C-regulated manner in stably transfected PC12 cell lines. J Biol Chem. 2003 Jun 13;278(24):22168–74. doi:10.1074/jbc.M301845200 PubMed PMID: 12682063; PubMed Central PMCID: PMC2597781.

39. Rothman RB, Baumann MH, Dersch CM, Romero DV, Rice KC, Carroll FI, et al. Amphetamine-type central nervous system stimulants release norepinephrine more potently than they release dopamine and serotonin. Synapse. 2001 Jan;39(1):32–41. doi:10.1002/1098-2396(20010101)39:1<32::AID-SYN5>3.0.CO;2-3 PubMed PMID: 11071707.

40. G R, Sc W. The molecular mechanism of "ecstasy" [3,4-methylenedioxy-methamphetamine (MDMA)]: serotonin transporters are targets for MDMA-induced serotonin release. Proceedings of the National Academy of Sciences of the United States of America. 1992 Jan 3;89(5). doi:10.1073/pnas.89.5.1817 PubMed PMID: 1347426.

41. Rickli A, Kopf S, Hoener MC, Liechti ME. Pharmacological profile of novel psychoactive benzofurans. British Journal of Pharmacology. 2015;172(13):3412–25. doi:10.1111/bph.13128

42. Simmler L, Buser T, Donzelli M, Schramm Y, Dieu LH, Huwyler J, et al. Pharmacological characterization of designer cathinones in vitro. British Journal of Pharmacology. 2013;168(2):458–70. doi:10.1111/j.1476-5381.2012.02145.x

43. Rios SM, Mootz JRK, Phillips TJ, Ingram SL. Absence of TAAR1 function increases methamphetamine-induced excitability of dorsal raphe serotonin neurons and drives binge-level methamphetamine intake. Neuropsychopharmacol. 2025 Jun;50(7):1136–44. doi:10.1038/s41386-025-02063-w

44. Huey JK, Shi X, Schutzer WE, Janowsky A, Abbas AI. Trace amine–associated receptor 1 agonists differentially regulate dopamine transporter function. Molecular Pharmacology. 2025 Sep 1;107(9). doi:10.1016/j.molpha.2025.100064 PubMed PMID: 40840012.

45. Ritz MC, Kuhar MJ. Relationship between self-administration of amphetamine and monoamine receptors in brain: comparison with cocaine. The Journal of Pharmacology and

Experimental Therapeutics. 1989 Mar 1;248(3):1010–7. doi:10.1016/S0022-3565(25)24116-7

46. Setola V, Hufeisen SJ, Grande-Allen KJ, Vesely I, Glennon RA, Blough B, et al. 3,4-methylenedioxymethamphetamine (MDMA, "Ecstasy") induces fenfluramine-like proliferative actions on human cardiac valvular interstitial cells in vitro. Mol Pharmacol. 2003 Jun;63(6):1223–9. doi:10.1124/mol.63.6.1223 PubMed PMID: 12761331.

47. Nash JF, Roth BL, Brodkin JD, Nichols DE, Gudelsky GA. Effect of the R(-) and S(+) isomers of MDA and MDMA on phosphatidyl inositol turnover in cultured cells expressing 5-HT2A or 5-HT2C receptors. Neurosci Lett. 1994 Aug 15;177(1–2):111–5. doi:10.1016/0304-3940(94)90057-4 PubMed PMID: 7824160.

48. AlOtaibi SD, Elsisi HA, AlShammary MJ, AlQader SA, AlHarbi HA, AlOlaiyan BR, et al. Evaluation of the Psychiatric Disorders among Amphetamine Addicts in Rehabilitation Centers: A Cross-Sectional Analysis. Journal of Toxicology. 2024 Jan 1;2024(1):1643693. doi:10.1155/2024/1643693

49. Paz-Ramos MI, Cruz SL, Violante-Soria V. Amphetamine-type Stimulants: Novel Insights into their Actions and use Patterns. Revista de Investigación Clínica. 2023 May 1;75(3):143–57. doi:10.24875/RIC.23000110

50. Darie IF, Praisler M, Negoita C. 2C-x and DOx hallucinogens: a systematic review. Analele Universității "Dunărea de Jos" din Galați Fascicula II, Matematică, fizică, mecanică teoretică / Annals of the "Dunarea de Jos" University of Galati Fascicle II, Mathematics, Physics, Theoretical Mechanics. 2021 Nov 12;44(1):46–52. doi:10.35219/ann-ugal-math-phys-mec.2021.1.07

51. Straumann I, Vizeli P, Avedisian I, Erne L, Noorshams D, Vukalovic I, et al. Acute effects of MDMA, MDA, lysine-MDMA, and lysine-MDA in a randomized, double-blind, placebo-controlled, crossover trial in healthy participants. Neuropsychopharmacol. 2025 Sep 25;1–10. doi:10.1038/s41386-025-02248-3

52. Stocker K, Liechti ME. Methylenedioxymethamphetamine is a connectogen with empathogenic, entactogenic, and still further connective properties: It is time to reconcile "the great entactogen—empathogen debate." J Psychopharmacol. 2024 Aug;38(8):685–9. doi:10.1177/02698811241265352 PubMed PMID: 39068642; PubMed Central PMCID: PMC11311894.

53. Hysek CM, Schmid Y, Simmler LD, Domes G, Heinrichs M, Eisenegger C, et al. MDMA enhances emotional empathy and prosocial behavior. Soc Cogn Affect Neurosci. 2014 Nov;9(11):1645–52. doi:10.1093/scan/nst161 PubMed PMID: 24097374; PubMed Central PMCID: PMC4221206.

54. Green AR, Mechan AO, Elliott JM, O'Shea E, Colado MI. The Pharmacology and Clinical Pharmacology of 3,4-Methylenedioxymethamphetamine (MDMA, "Ecstasy"). Pharmacological Reviews. 2003 Sep 1;55(3):463–508. doi:10.1124/pr.55.3.3

55. Montgomery T, Buon C, Eibauer S, Guiry PJ, Keenan AK, McBean GJ. Comparative potencies of 3,4-methylenedioxymethamphetamine (MDMA) analogues as inhibitors of [3H]noradrenaline and [3H]5-HT transport in mammalian cell lines. British Journal of Pharmacology. 2007;152(7):1121–30. doi:10.1038/sj.bjp.0707473

56. Alberto-Silva AS, Hemmer S, Bock HA, da Silva LA, Scott KR, Kastner N, et al. Bioisosteric analogs of MDMA: improving the pharmacological profile? J Neurochem. 2024 Sep;168(9):2022–42. doi:10.1111/jnc.16149 PubMed PMID: 38898705; PubMed Central PMCID: PMC11449655.

57. Liechti ME, Baumann C, Gamma A, Vollenweider FX. Acute Psychological Effects of 3,4-Methylenedioxymethamphetamine (MDMA, "Ecstasy") are Attenuated by the Serotonin Uptake Inhibitor Citalopram. Neuropsychopharmacol. 2000 May;22(5):513–21. doi:10.1016/S0893-133X(99)00148-7

58. Liechti ME, Vollenweider FX. The serotonin uptake inhibitor citalopram reduces acute cardiovascular and vegetative effects of 3,4-methylenedioxymethamphetamine ('Ecstasy') in healthy volunteers. J Psychopharmacol. 2000;14(3):269–74. doi:10.1177/026988110001400313 PubMed PMID: 11106307.

59. Hysek C, Simmler L, Ineichen M, Grouzmann E, Hoener M, Brenneisen R, et al. The Norepinephrine Transporter Inhibitor Reboxetine Reduces Stimulant Effects of MDMA ("Ecstasy") in Humans. Clinical Pharmacology & Therapeutics. 2011;90(2):246–55. doi:10.1038/clpt.2011.78

60. Baumann MH, Ayestas MA, Partilla JS, Sink JR, Shulgin AT, Daley PF, et al. The Designer Methcathinone Analogs, Mephedrone and Methylone, are Substrates for Monoamine Transporters in Brain Tissue. Neuropsychopharmacol. 2012 Apr;37(5):1192–203. doi:10.1038/npp.2011.304

61. Wee S, Anderson KG, Baumann MH, Rothman RB, Blough BE, Woolverton WL. Relationship between the Serotonergic Activity and Reinforcing Effects of a Series of Amphetamine Analogs. The Journal of Pharmacology and Experimental Therapeutics. 2005 May 1;313(2):848–54. doi:10.1124/jpet.104.080101

62. Pomrenze MB, Vaillancourt S, Salgado JS, Raymond KB, Llorach P, Sacai H, et al. 5-HT2C receptors in the nucleus accumbens constrain the rewarding effects of MDMA. Mol Psychiatry. 2025 Jul 24;1–12. doi:10.1038/s41380-025-03128-4

63. Thompson MR, Callaghan PD, Hunt GE, Cornish JL, McGregor IS. A role for oxytocin and 5-HT(1A) receptors in the prosocial effects of 3,4 methylenedioxymethamphetamine ("ecstasy"). Neuroscience. 2007 May 11;146(2):509–14. doi:10.1016/j.neuroscience.2007.02.032 PubMed PMID: 17383105.

64. Dumont GJH, Sweep FCGJ, van der Steen R, Hermsen R, Donders ART, Touw DJ, et al. Increased oxytocin concentrations and prosocial feelings in humans after ecstasy (3,4-methylenedioxymethamphetamine) administration. Social Neuroscience. 2009 Aug 1;4(4):359–66. doi:10.1080/17470910802649470 PubMed PMID: 19562632.

65. Donaldson ZR, Young LJ. Oxytocin, Vasopressin, and the Neurogenetics of Sociality. Science. 2008 Nov 7;322(5903):900–4. doi:10.1126/science.1158668

66. De Dreu CKW, Greer LL, Handgraaf MJJ, Shalvi S, Van Kleef GA, Baas M, et al. The neuropeptide oxytocin regulates parochial altruism in intergroup conflict among humans. Science. 2010 Jun 11;328(5984):1408–11. doi:10.1126/science.1189047 PubMed PMID: 20538951.

67. Francis SM, Kirkpatrick MG, de Wit H, Jacob S. Urinary and plasma oxytocin changes in response to MDMA or intranasal oxytocin administration. Psychoneuroendocrinology. 2016 Dec 1;74:92–100. doi:10.1016/j.psyneuen.2016.08.011

68. Heifets BD, Salgado JS, Taylor MD, Hoerbelt P, Pinto DFC, Steinberg EE, et al. Distinct neural mechanisms for the prosocial and rewarding properties of MDMA. Sci Transl Med. 2019 Dec 11;11(522):eaaw6435. doi:10.1126/scitranslmed.aaw6435 PubMed PMID: 31826983; PubMed Central PMCID: PMC7123941.

69. Hysek C, Schmid Y, Rickli A, Simmler LD, Donzelli M, Grouzmann E, et al. Carvedilol inhibits the cardiostimulant and thermogenic effects of MDMA in humans. Br J Pharmacol. 2012 Aug;166(8):2277–88. doi:10.1111/j.1476-5381.2012.01936.x PubMed PMID: 22404145; PubMed Central PMCID: PMC3448893.

70. de la Torre R, Farré M, Ortuño J, Mas M, Brenneisen R, Roset PN, et al. Non-linear pharmacokinetics of MDMA ('ecstasy') in humans. Br J Clin Pharmacol. 2000 Feb;49(2):104–9. doi:10.1046/j.1365-2125.2000.00121.x PubMed PMID: 10671903; PubMed Central PMCID: PMC2014905.

71. Wu D, Otton SV, Inaba T, Kalow W, Sellers EM. Interactions of amphetamine analogs with human liver CYP2D6. Biochem Pharmacol. 1997 Jun 1;53(11):1605–12. doi:10.1016/s0006-2952(97)00014-2 PubMed PMID: 9264312.

72. Baumann MH, Zolkowska D, Kim I, Scheidweiler KB, Rothman RB, Huestis MA. Effects of Dose and Route of Administration on Pharmacokinetics of (±)-3,4-Methylenedioxymethamphetamine in the Rat. Drug Metab Dispos. 2009 Nov;37(11):2163–70. doi:10.1124/dmd.109.028506 PubMed PMID: 19679675; PubMed Central PMCID: PMC2774984.

73. Stone DM, Hanson GR, Gibb JW. Differences in the central serotonergic effects of methylenedioxymethamphetamine (MDMA) in mice and rats. Neuropharmacology. 1987 Nov;26(11):1657–61. doi:10.1016/0028-3908(87)90017-7 PubMed PMID: 2448703.

74. Logan BJ, Laverty R, Sanderson WD, Yee YB. Differences between rats and mice in MDMA (methylenedioxymethylamphetamine) neurotoxicity. Eur J Pharmacol. 1988 Aug 2;152(3):227–34. doi:10.1016/0014-2999(88)90717-0 PubMed PMID: 2906000.

75. Reveron ME, Monks TJ, Duvauchelle CL. Age-dependent (+)MDMA-mediated neurotoxicity in mice. Neurotoxicology. 2005 Dec;26(6):1031–40. doi:10.1016/j.neuro.2005.05.006 PubMed PMID: 15998542.

76. Costa G, Porceddu PF, Serra M, Casu MA, Schiano V, Napolitano F, et al. Lack of Rhes Increases MDMA-Induced Neuroinflammation and Dopamine Neuron Degeneration: Role of Gender and Age. Int J Mol Sci. 2019 Mar 28;20(7):1556. doi:10.3390/ijms20071556 PubMed PMID: 30925704; PubMed Central PMCID: PMC6480667.

77. Chen Y, Tran HTN, Saber YH, Hall FS. High ambient temperature increases the toxicity and lethality of 3,4-methylenedioxymethamphetamine and methcathinone. Pharmacol Biochem Behav. 2020 May;192:172912. doi:10.1016/j.pbb.2020.172912 PubMed PMID: 32201298; PubMed Central PMCID: PMC7294679.

78. Pardo-Lozano R, Farré M, Yubero-Lahoz S, O'Mathúna B, Torrens M, Mustata C, et al. Clinical pharmacology of 3,4-methylenedioxymethamphetamine (MDMA, "ecstasy"): the influence of gender and genetics (CYP2D6, COMT, 5-HTT). PLoS One. 2012;7(10):e47599. doi:10.1371/journal.pone.0047599 PubMed PMID: 23112822; PubMed Central PMCID: PMC3480420.

79. Neurotoxicity of MDMA and Related Compounds: Anatomic Studiesa - MOLLIVER - 1990 - Annals of the New York Academy of Sciences - Wiley Online Library [Internet]. [cited 2025 Sep 18]. Available from: https://nyaspubs.onlinelibrary.wiley.com/doi/10.1111/j.1749-6632.1990.tb16916.x

80. Baumann MH, Wang X, Rothman RB. 3,4-Methylenedioxymethamphetamine (MDMA) neurotoxicity in rats: a reappraisal of past and present findings. Psychopharmacology (Berl). 2007;189:407–24. doi:10.1007/s00213-006-0322-6 PubMed PMID: 16541247; PubMed Central PMCID: PMC1705495.

81. Müller F, Brändle R, Liechti ME, Borgwardt S. Neuroimaging of chronic MDMA ("ecstasy") effects: A meta-analysis. Neuroscience & Biobehavioral Reviews. 2019 Jan 1;96:10–20. doi:10.1016/j.neubiorev.2018.11.004

82. Buchert R, Thomasius R, Petersen K, Wilke F, Obrocki J, Nebeling B, et al. Reversibility of ecstasy-induced reduction in serotonin transporter availability in polydrug ecstasy users. Eur J Nucl Med Mol Imaging. 2006 Feb 1;33(2):188–99. doi:10.1007/s00259-005-1850-8

83. Reneman L, Lavalaye J, Schmand B, de Wolff FA, van den Brink W, den Heeten GJ, et al. Cortical serotonin transporter density and verbal memory in individuals who stopped using 3,4-methylenedioxymethamphetamine (MDMA or "ecstasy"): preliminary findings. Arch Gen Psychiatry. 2001 Oct;58(10):901–6. doi:10.1001/archpsyc.58.10.901 PubMed PMID: 11576026.

84. Selvaraj S, Hoshi R, Bhagwagar Z, Murthy NV, Hinz R, Cowen P, et al. Brain serotonin transporter binding in former users of MDMA ('ecstasy'). Br J Psychiatry. 2009 Apr;194(4):355–9. doi:10.1192/bjp.bp.108.050344 PubMed PMID: 19336788.

85. Pantoni MM, Anagnostaras SG. Cognitive Effects of MDMA in Laboratory Animals: A Systematic Review Focusing on Dose. Pharmacol Rev. 2019 Jul;71(3):413–49. doi:10.1124/pr.118.017087 PubMed PMID: 31249067; PubMed Central PMCID: PMC6607799.

86. Fox HC, Parrott AC, Turner JJ. Ecstasy use: cognitive deficits related to dosage rather than self-reported problematic use of the drug. J Psychopharmacol. 2001 Dec;15(4):273–81. doi:10.1177/026988110101500406 PubMed PMID: 11769821.

87. Costa G, Gołembiowska K. Neurotoxicity of MDMA: Main effects and mechanisms. Experimental Neurology. 2022 Jan 1;347:113894. doi:10.1016/j.expneurol.2021.113894

88. López-Arnau R, Martínez-Clemente J, Pubill D, Escubedo E, Camarasa J. Comparative neuropharmacology of three psychostimulant cathinone derivatives: butylone, mephedrone and methylone. Br J Pharmacol. 2012 Sep;167(2):407–20. doi:10.1111/j.1476-5381.2012.01998.x PubMed PMID: 22509960; PubMed Central PMCID: PMC3481047.

89. Baarset AM, Steinsland S, Nerem E, Andersen JM, Baumann MH, Bogen IL. Pharmacological effects and pharmacokinetics of the novel synthetic cathinone α-pyrrolidinoisohexanophenone (α-PiHP) compared with α-pyrrolidinovalerophenone (α-PVP) in mice. NeuroToxicology. 2025 May 1;108:412–21. doi:10.1016/j.neuro.2025.05.005

90. Saha K, Partilla JS, Lehner KR, Seddik A, Stockner T, Holy M, et al. 'Second-Generation' Mephedrone Analogs, 4-MEC and 4-MePPP, Differentially Affect Monoamine Transporter Function. Neuropsychopharmacol. 2015 May;40(6):1321–31. doi:10.1038/npp.2014.325

91. Monte AP, Marona-Lewicka D, Cozzi NV, Nichols DE. Synthesis and pharmacological examination of benzofuran, indan, and tetralin analogs of 3,4-(methylenedioxy)amphetamine. J Med Chem. 1993 Nov 1;36(23):3700–6. doi:10.1021/jm00075a027

92. Drugs-Forum [Internet]. 2013 [cited 2025 Sep 22]. Drug information - 5-EAPB (1-(benzofuran-5-yl)-N-ethylpropan-2-amine) Drug Info. Available from: https://drugs-forum.com/threads/5-eapb-1-benzofuran-5-yl-n-ethylpropan-2-amine-drug-info.217991/

93. Bluelight.org [Internet]. 2013 [cited 2025 Sep 22]. The Main 5-APDB Thread. Available from: https://www.bluelight.org/community/threads/the-main-5-apdb-thread.672585/

94. Bluelight.org [Internet]. 2013 [cited 2025 Sep 22]. The Main 6-APDB Thread. Available from: https://www.bluelight.org/community/threads/the-main-6-apdb-thread.661435/

95. Bhattacharyya S, Schapira AH, Mikhailidis DP, Davar J. Drug-induced fibrotic valvular heart disease. The Lancet. 2009 Aug 15;374(9689):577–85. doi:10.1016/S0140-6736(09)60252-X PubMed PMID: 19683643.

96. Eshleman AJ, Wolfrum KM, Hatfield MG, Johnson RA, Murphy KV, Janowsky A. Substituted methcathinones differ in transporter and receptor interactions. Biochem Pharmacol. 2013 Jun 15;85(12):1803–15. doi:10.1016/j.bcp.2013.04.004 PubMed PMID: 23583454; PubMed Central PMCID: PMC3692398.

97. Cozzi NV, Sievert MK, Shulgin AT, Jacob P, Ruoho AE. Inhibition of plasma membrane monoamine transporters by β-ketoamphetamines. European Journal of Pharmacology. 1999 Sep 17;381(1):63–9. doi:10.1016/S0014-2999(99)00538-5

98. Silva-Carvalho M, Barbosa DJ, Dias da Silva D, Dinis-Oliveira RJ. Multidimensional Evaluation of Lisdexamfetamine: Pharmacology, Therapeutic Use, Toxicity and Forensic Implications. Basic Clin Pharmacol Toxicol. 2025 Nov;137(5):e70111. doi:10.1111/bcpt.70111 PubMed PMID: 41001763; PubMed Central PMCID: PMC12464896.

99. PharmaWiki - Adderall® [Internet]. [cited 2025 Sep 29]. Available from: https://www.pharmawiki.ch/wiki/index.php?wiki=Adderall

100. Black SW, Yamanaka A, Kilduff TS. Challenges in the development of therapeutics for narcolepsy. Prog Neurobiol. 2017 May;152:89–113. doi:10.1016/j.pneurobio.2015.12.002 PubMed PMID: 26721620; PubMed Central PMCID: PMC5114175.

101. Bupropion Sandoz 150 mg - Tablette mit veränderter Wirkstofffreisetzung - Zusammengefasste Informationen | Info Patient [Internet]. [cited 2025 Sep 29]. Available

from: https://info-patient.at/bupropion-sandoz-150-mg-tablette-mit-veraenderter-wirkstofffreisetzung-103524/zusammenfassende-informationen

102. Oldak SE, Maristany AJ. Bupropion and Anxiety: A Brief Review. Hum Psychopharmacol. 2025 Sep;40(5):e70018. doi:10.1002/hup.70018 PubMed PMID: 40958494.

103. Tønnesen P, Tonstad S, Hjalmarson A, Lebargy F, Van Spiegel PI, Hider A, et al. A multicentre, randomized, double-blind, placebo-controlled, 1-year study of bupropion SR for smoking cessation. J Intern Med. 2003 Aug;254(2):184–92. doi:10.1046/j.1365-2796.2003.01185.x PubMed PMID: 12859700.

104. Junkes L, Quagliato LA, Appolinario JC, Shader RI, Nardi AE. MAO inhibitors for treatment-resistant depression: Bringing an updated perspective on pioneering drugs. Pharmacological Research. 2025 Sep 1;219:107876. doi:10.1016/j.phrs.2025.107876

105. Galli S, Pacilio P, Bianchini E, Alborghetti M, De Carolis L, Lombardo P, et al. The Role of MAO-B Inhibitors in Fatigue in Parkinson's Disease: A Narrative Review. J Clin Med. 2025 Apr 10;14(8):2598. doi:10.3390/jcm14082598 PubMed PMID: 40283428; PubMed Central PMCID: PMC12027954.

106. Semmlinger V, Leithner C, Klöck LM, Ranftl L, Ehring T, Schreckenbach M. Prevalence and Predictors of Nonresponse to Psychological Treatment for PTSD: A Meta-Analysis. Depress Anxiety. 2024 Jul 26;2024:9899034. doi:10.1155/2024/9899034 PubMed PMID: 40226730; PubMed Central PMCID: PMC11918500.

107. Mitchell JM, Ot'alora G. M, van der Kolk B, Shannon S, Bogenschutz M, Gelfand Y, et al. MDMA-assisted therapy for moderate to severe PTSD: a randomized, placebo-controlled phase 3 trial. Nat Med. 2023 Oct;29(10):2473–80. doi:10.1038/s41591-023-02565-4

108. Mitchell JM, Bogenschutz M, Lilienstein A, Harrison C, Kleiman S, Parker-Guilbert K, et al. MDMA-assisted therapy for severe PTSD: a randomized, double-blind, placebo-controlled phase 3 study. Nat Med. 2021 Jun;27(6):1025–33. doi:10.1038/s41591-021-01336-3 PubMed PMID: 33972795; PubMed Central PMCID: PMC8205851.

109. Young MB, Norrholm SD, Khoury LM, Jovanovic T, Rauch SAM, Reiff CM, et al. Inhibition of serotonin transporters disrupts the enhancement of fear memory extinction by 3,4-methylenedioxymethamphetamine (MDMA). Psychopharmacology (Berl). 2017 Oct;234(19):2883–95. doi:10.1007/s00213-017-4684-8 PubMed PMID: 28741031; PubMed Central PMCID: PMC5693755.

110. Young MB, Andero R, Ressler KJ, Howell LL. 3,4-Methylenedioxymethamphetamine facilitates fear extinction learning. Transl Psychiatry. 2015 Sep;5(9):e634. doi:10.1038/tp.2015.138 PubMed PMID: 26371762; PubMed Central PMCID: PMC5068803.

111. Hake HS, Davis JKP, Wood RR, Tanner M, Loetz EC, Sanchez A, et al. 3,4-methylenedioxymethamphetamine (MDMA) impairs the extinction and reconsolidation of fear memory in rats. Physiol Behav. 2019 Feb 1;199:343–50. doi:10.1016/j.physbeh.2018.12.007 PubMed PMID: 30529341; PubMed Central PMCID: PMC6557441.

112. Doss MK, Weafer J, Gallo DA, de Wit H. MDMA Impairs Both the Encoding and Retrieval of Emotional Recollections. Neuropsychopharmacol. 2018 Mar;43(4):791–800. doi:10.1038/npp.2017.171

113. Tan E, Chin CSH, Lim ZFS, Ng SK. HEK293 Cell Line as a Platform to Produce Recombinant Proteins and Viral Vectors. Front Bioeng Biotechnol. 2021 Dec 13;9:796991. doi:10.3389/fbioe.2021.796991 PubMed PMID: 34966729; PubMed Central PMCID: PMC8711270.

114. Sucic S, Bönisch H. Classical Radioligand Uptake and Binding Methods in Transporter Research: An Emphasis on the Monoamine Neurotransmitter Transporters. In: Bönisch H, Sitte HH, editors. Neurotransmitter Transporters: Investigative Methods [Internet]. New York, NY: Springer; 2016 [cited 2025 Nov 11]. p. 1–21. Available from: https://doi.org/10.1007/978-1-4939-3765-3_1 doi:10.1007/978-1-4939-3765-3_1

115. Mayer FP, Luf A, Nagy C, Holy M, Schmid R, Freissmuth M, et al. Application of a Combined Approach to Identify New Psychoactive Street Drugs and Decipher Their Mechanisms at Monoamine Transporters. In: Baumann MH, Glennon RA, Wiley JL, editors. Neuropharmacology of New Psychoactive Substances (NPS): The Science Behind the Headlines [Internet]. Cham: Springer International Publishing; 2017 [cited 2025 Nov 10]. p. 333–50. Available from: https://doi.org/10.1007/7854_2016_63 doi:10.1007/7854_2016_63

116. Baumann MH, Partilla JS, Lehner KR, Thorndike EB, Hoffman AF, Holy M, et al. Powerful Cocaine-Like Actions of 3,4-Methylenedioxypyrovalerone (MDPV), a Principal Constituent of Psychoactive 'Bath Salts' Products. Neuropsychopharmacology. 2013 Mar;38(4):552–62. doi:10.1038/npp.2012.204 PubMed PMID: 23072836; PubMed Central PMCID: PMC3572453.

117. Steinkellner T, Mayer FP, Hofmaier T, Holy M, Montgomery T, Eisenrauch B, et al. Tracer Flux Measurements to Study Outward Transport by Monoamine Neurotransmitter Transporters. In: Bönisch H, Sitte HH, editors. Neurotransmitter Transporters: Investigative Methods [Internet]. New York, NY: Springer; 2016 [cited 2025 Nov 11]. p. 23–40. Available from: https://doi.org/10.1007/978-1-4939-3765-3_2 doi:10.1007/978-1-4939-3765-3_2

118. Seidel S, Singer EA, Just H, Farhan H, Scholze P, Kudlacek O, et al. Amphetamines take two to tango: an oligomer-based counter-transport model of neurotransmitter transport explores the amphetamine action. Mol Pharmacol. 2005 Jan;67(1):140–51. doi:10.1124/mol.67.1. PubMed PMID: 15615700.

119. Nadal-Gratacós N, Alberto-Silva AS, Rodríguez-Soler M, Urquizu E, Espinosa-Velasco M, Jäntsch K, et al. Structure–Activity Relationship of Novel Second-Generation Synthetic Cathinones: Mechanism of Action, Locomotion, Reward, and Immediate-Early Genes. Front Pharmacol. 2021 Oct 26;12. doi:10.3389/fphar.2021.749429

120. Brugnoli FR, Holy M, Niello M, Maier J, Hanreich M, Menzel M, et al. Development and validation of an automated microfluidic perfusion platform for parallelized screening of compounds in vitro. Basic & Clinical Pharmacology & Toxicology. 2023;133(5):535–47. doi:10.1111/bcpt.13940

121. Administration (TGA) TG. Update on MDMA and psilocybin access and safeguards from 1 July 2023 | Therapeutic Goods Administration (TGA) [text] [Internet]. Therapeutic Goods Administration (TGA); 2023 [cited 2026 May 20]. Available from:

https://www.tga.gov.au/news/news-articles/update-mdma-and-psilocybin-access-and-safeguards-1-july-2023

122. Liechti ME, Gasser P, Aicher HD, Mueller F, Hawrot T, Schmid Y. Implementing psychedelic-assisted therapy: History and characteristics of the Swiss limited medical use program. Neuroscience Applied. 2025 Jan 1;4:105525. doi:10.1016/j.nsa.2025.105525

123. Begrenzte medizinische Verwendung verbotener Betäubungsmittel [Internet]. [cited 2026 May 25]. Available from: https://www.bag.admin.ch/en/limited-medical-use-of-banned-narcotics#Requirements-for-limited-medical-use-of-bannednarcotics

124. Johnson CB, Walther D, Baggott MJ, Baker LE, Baumann MH. Novel Benzofuran Derivatives Induce Monoamine Release and Substitute for the Discriminative Stimulus Effects of 3,4-Methylenedioxymethamphetamine. J Pharmacol Exp Ther. 2024 Oct;391(1):22–9. doi:10.1124/jpet.123.001837 PubMed PMID: 38272669; PubMed Central PMCID: PMC11413916.

125. Neumann J, Hußler W, Hofmann B, Gergs U. Contractile Effects of Amphetamine, Pseudoephedrine, Nor-pseudoephedrine (Cathine), and Cathinone on Atrial Preparations of Mice and Humans. Journal of Cardiovascular Pharmacology. 2024 Mar;83(3):243. doi:10.1097/FJC.0000000000001536

126. Heisinger S. Pharmacological characterization of New Psychoactive Substances [Internet]. 2025 [cited 2026 Feb 15]. Available from: http://pub.hcw.ac.at/obvfcwhsacc/11697027

127. Eshleman AJ, Nagarajan S, Wolfrum KM, Reed JF, Swanson TL, Nilsen A, et al. Structure-activity relationships of bath salt components: substituted cathinones and benzofurans at biogenic amine transporters. Psychopharmacology (Berl). 2019 Mar;236(3):939–52. doi:10.1007/s00213-018-5059-5 PubMed PMID: 30397775; PubMed Central PMCID: PMC6500773.

128. Scholze P, Sitte HH, Singer EA. Substantial loss of substrate by diffusion during uptake in HEK-293 cells expressing neurotransmitter transporters. Neurosci Lett. 2001 Aug 31;309(3):173–6. doi:10.1016/s0304-3940(01)02058-4 PubMed PMID: 11514069.

129. Brandt SD, Walters HM, Partilla JS, Blough BE, Kavanagh PV, Baumann MH. The psychoactive aminoalkylbenzofuran derivatives, 5-APB and 6-APB, mimic the effects of 3,4-methylenedioxyamphetamine (MDA) on monoamine transmission in male rats. Psychopharmacology (Berl). 2020 Dec;237(12):3703–14. doi:10.1007/s00213-020-05648-z PubMed PMID: 32875347; PubMed Central PMCID: PMC7686291.

130. Hasenhuetl PS, Bhat S, Freissmuth M, Sandtner W. Functional Selectivity and Partial Efficacy at the Monoamine Transporters: A Unified Model of Allosteric Modulation and Amphetamine-Induced Substrate Release. Molecular Pharmacology. 2019 Mar 1;95(3):303–12. doi:10.1124/mol.118.114793

131. Möller IR, Slivacka M, Nielsen AK, Rasmussen SGF, Gether U, Loland CJ, et al. Conformational dynamics of the human serotonin transporter during substrate and drug binding. Nat Commun. 2019 Apr 11;10(1):1687. doi:10.1038/s41467-019-09675-z PubMed PMID: 30976000; PubMed Central PMCID: PMC6459873.

132. Mayer FP, Niello M, Bulling S, Zhang YW, Li Y, Kudlacek O, et al. Mephedrone induces partial release at human dopamine transporters but full release at human serotonin transporters. Neuropharmacology. 2023 Dec 1;240:109704. doi:10.1016/j.neuropharm.2023.109704

133. Schmitt KC, Rothman RB, Reith MEA. Nonclassical Pharmacology of the Dopamine Transporter: Atypical Inhibitors, Allosteric Modulators, and Partial Substrates. J Pharmacol Exp Ther. 2013 Jul;346(1):2–10. doi:10.1124/jpet.111.191056 PubMed PMID: 23568856; PubMed Central PMCID: PMC3684841.

# 7 Appendix

## 7.1 Zusammenfassung

Neue psychoaktive Substanzen gewinnen zunehmend an Bedeutung im Bereich der öffentlichen Gesundheit und könnten neue therapeutische Ansätze für psychiatrische und kognitive Störungen ermöglichen. MDMA wird derzeit in Phase-3-Studien als Ergänzung zur Psychotherapie zur Behandlung von PTBS untersucht. Nach zwei Phase-3-Studien forderte die FDA in einem *Complete Response Letter* weitere Untersuchungen zur Sicherheit und Wirksamkeit. Dies führte zur Entwicklung von MDMA-Analoga mit potenziell verbesserten pharmakologischen Profilen.

In dieser Masterarbeit wurden sechs Benzofurancathinon-Derivate *in vitro* hinsichtlich ihrer Aktivität an den Monoamintransportern SERT, DAT und NET untersucht. Hierzu wurden Wiederaufnahmehemmungs- und superfusionsbasierte Freisetzungsassays in HEK-293-Zellen durchgeführt und $IC_{50}$-Werte sowie Freisetzungseigenschaften bestimmt.

Die Ergebnisse zeigten, dass Stereochemie, Substituentenposition am Benzofuranring und Alkylkettenlänge die $IC_{50}$ Werte beeinflussen. Die Potenz variierte zwischen den Transportern mit der höchsten Potenz am DAT, gefolgt von NET und SERT. Alle untersuchten Substanzen induzierten Freisetzung an SERT. Am DAT wurde Freisetzung nur für *R*-βK-6-MAPB beobachtet, während am NET beide Stereoisomere von βK-6-MAPB Freisetzung zeigten.

Diese Ergebnisse deuten darauf hin, dass ausgewählte Benzofurancathinone eine selektive serotonerge Aktivität aufweisen könnten und somit potenziell vielversprechende Kandidaten für eine weitere pharmakologische Evaluierung in der Behandlung von PTBS darstellen.